The Astrophysical Journal, 591:695–713, 2003 July 10
© 2003. The American Astronomical Society. All rights reserved. Printed in U.S.A.

THE CROSS-WAVELET TRANSFORM AND ANALYSIS OF QUASI-PERIODIC BEHAVIOR IN THE PEARSON-READHEAD VLBI SURVEY SOURCES

Brandon C. Kelly, Philip A. Hughes, Hugh D. Aller, and Margo F. Aller
Astronomy Department, University of Michigan, Ann Arbor, MI 48109-1090; bckelly@umich.edu, hughes@astro.lsa.umich.edu, hugh@astro.lsa.umich.edu, margo@astro.lsa.umich.edu
Received 2002 September 6; accepted 2003 March 24

ABSTRACT

We introduce an algorithm for applying a cross-wavelet transform to analysis of quasi-periodic variations in a time series and introduce significance tests for the technique. We apply a continuous wavelet transform and the cross-wavelet algorithm to the Pearson-Readhead VLBI survey sources using data obtained from the University of Michigan 26 m paraboloid at observing frequencies of 14.5, 8.0, and 4.8 GHz. Thirty of the 62 sources were chosen to have sufficient data for analysis, having at least 100 data points for a given time series. Of these 30 sources, a little more than half exhibited evidence for quasi-periodic behavior in at least one observing frequency, with a mean characteristic period of 2.4 yr and standard deviation of 1.3 yr. We find that out of the 30 sources, there were about four timescales for every 10 time series, and about half of those sources showing quasi-periodic behavior repeated the behavior in at least one other observing frequency.

Subject headings: galaxies: active — galaxies: jets — galaxies:nuclei — methods: data analysis — radio continuum: galaxies

On-line material: color figures

1. INTRODUCTION

It is well accepted that centimeter wave band emission from active galactic nuclei is associated with a jet of synchrotron plasma, the accretion structure and immediate environment of a supermassive black hole contributing broadband emission from the infrared to the gamma-ray spectrum. Temporal variations are observed in the radio flux, and a number of processes have been proposed to explain this, such as an accretion rate that may change with time, an accretion disk that exhibits instability, an outflow that may be Kelvin-Helmholtz unstable, or an outflow that may interact with ambient inhomogeneities. The temporal variations in the radio flux motivate a search for characteristic timescales and, if found, would lend insight into the mechanisms causing the variations.

In practice, searching for possible quasi-periodic behavior masked by a stochastic component can be rather difficult, especially in the context of irregular time sampling. One promising technique is to perform a continuous wavelet transform on the signal and map out the coefficients in wavelet space. This was done on data for the BL Lac object OJ 287, resulting in evidence for periods in the radio spectral region of $\sim$1.66 yr, with $\sim$1.12 yr dominating in the 1980s (Hughes, Aller, & Aller 1998). The results led Hughes et al. (1998) to propose that the results can best be explained by a "shock-in-jet" model, in which the longer periodicity is linked with an otherwise quiescent jet, and the shorter with a passing shock wave.

The continuous wavelet transform detects quasi-periodic behavior through visual examination of the map over translation and dilation and assigns a characteristic timescale by looking for peaks in the time-averaged wavelet power (see § 4.1). The scales that the peaks occur at correspond to Fourier periods, from which a characteristic timescale can be deduced. Although the continuous transform is effective, when assigning a characteristic timescale it does not fully include information on how a time series varies in dilation; the timescale corresponds to those dilations where the time-averaged wavelet power spectrum peaks. In order to use all of the available information in the transform, we examine the cross-wavelet transform, in which the coefficients for the continuous transform of a signal are multiplied by the complex conjugate of the coefficients of another signal. The results are then mapped out in wavelet space and analyzed for correlation. A cross-wavelet analysis was used on the OJ 94 project light curve (Lehto 1999) and has seen application in other areas of science as well (Pancheva et al. 2000; Kyprianou & Staszewski 1999). We examine this method in greater depth, as well as a technique for finding the characteristic period of a signal, and apply this to the Pearson-Readhead (PR) VLBI survey sources using data from the University of Michigan Radio Astronomy Observatory (UMRAO) from three observing frequencies. The PR group is well suited for analyzing quasi-periodicity, because of the high signal-to-noise ratio (S/N) in the data for most of these sources (Aller, Aller, & Hughes 2003), as well as for investigating quasi-periodic variations (QPVs) as a function of optical source type, since it contains representatives from the optical classes QSO, galaxy, and BL Lac object. In addition, the time base of the UMRAO data is around 20 yr for most sources, allowing possible quasi-periodic events of as long as 4 yr to be observed for at least four to five cycles. Using UMRAO data, evidence has been found for periodic behavior in the centimeter wave band emission for the BL Lac object 0235+164 (Roy et al. 2000). However, there have not been any convincing indications of periodicity for PR sources (Aller et al. 2003).

2. THE DATA

The data for this study were acquired as part of the UMRAO program, using the University of Michigan 26 m paraboloid. Sixty-two of the 65 PR sources are within the declination limits of the paraboloid, and these sources have been observed at least trimonthly at 14.5, 8.0, and 4.8 GHz

since the fall of 1984, with occasional gaps due to poor weather and positions too near to the Sun to be observed. The observing technique and reduction procedures used are those described in Aller et al. (1985) and H. D. Aller et al. (2003, in preparation), with the latter including a rescaling of the data for the purpose of conforming with the flux system of Ott et al. (1994).

3. WAVELET TRANSFORMS

3.1. *The Continuous Wavelet Transform*

The continuous wavelet transform involves decomposing a signal $f(t)$ into a number of translated and dilated wavelets. The main idea behind this is to take a "mother" wavelet, translate and dilate it, convolve it with the function of interest, and map out the coefficients in "wavelet space," spanned by translation and dilation. Periodic behavior then shows up as a pattern spanning all translations at a given dilation, and this redundancy in the wavelet space makes detection of periodic behavior rather easy. The wavelet transform preserves temporal locality, which is an advantage over Fourier analysis. For instance, power associated with irregular sampling does not contribute to the coefficients as in Fourier analysis, which is extremely helpful when using poorly sampled data.

There are several common types of mother wavelets. In this analysis we use a Morlet wavelet of $k_\psi = 6$, given by

$$\psi_{\rm Morlet} = \pi^{-1/4} e^{-ik_\psi t} e^{-|t^2|/2} , \tag{1}$$

with coefficients

$$\tilde{f}(l,t') = \int_{\boldsymbol{R}} f(t)\psi^*_{lt'}(t)\,dt , \tag{2}$$

$$\psi_{lt'}(t) = \frac{1}{\sqrt{l}}\psi\left(\frac{t-t'}{l}\right) , \quad l \in \boldsymbol{R}^+ , \quad t \in \boldsymbol{R} . \tag{3}$$

The continuous transform must also satisfy an admissibility condition, requiring zero mean:

$$\int_{\boldsymbol{R}} \psi(t)\,dt = 0 . \tag{4}$$

It should be noted that l corresponds to dilations, and t' refers to translations. Generally, the parameter k_ψ remains fixed throughout the analysis and, for simplicity, is hereafter just k. Figure 1*a* shows the continuous wavelet transform for a sinusoidal signal. The periodic behavior is easily revealed by the redundancy in the plot. For the interested reader, more detailed information on the continuous wavelet transform may be found in Farge (1992).

3.2. *The Cross-Wavelet Transform*

The continuous wavelet transform is effective for examining how a time series varies in time and scale but fails to include how it varies over a range of scales when assigning a period that best characterizes it. After identifying that a periodic pattern exists in what can be potentially noisy and poorly sampled data, one finds the dilation that characterizes the period from the time-averaged data (i.e., the wavelet power spectrum), and from that dilation the period is calculated. For a quasi-periodic signal there is no unique dilation; there is a need for a method of directly measuring a characteristic timescale, or timescales, that includes information on how a source varies in dilation, and for this we examine the cross-wavelet transform.

Given two time series $f_a(t)$ and $f_m(t)$, we can construct the cross-wavelet transform

$$\tilde{f}_c(l,t') = \tilde{f}_a(l,t')\tilde{f}^*_m(l,t') , \tag{5}$$

where $\tilde{f}_a$ and $\tilde{f}_m$ are given by equation (2). In this analysis $f_a(t)$ is the source signal and $f_m(t)$ is a sinusoidal mock signal, although one can use any two time series thought to be correlated.

Because we are looking for quasi-periodic behavior, we first assume an ideal signal of the form

$$f_a(t) = A_a e^{i(\omega_a t+\phi_a)} , \quad -\infty < t < \infty , \tag{6}$$

where $\omega_a = 2\pi/\tau_a$ for period τ_a. Anticipating that it will be productive to cross the actual signal with a signal of a similar form, we try a mock signal

$$f_m(t) = A_m e^{i(\omega_m t+\phi_m)} , \quad -\infty < t < \infty . \tag{7}$$

Each of these signals will have continuous wavelet coefficients given by equation (2):

$$\tilde{f}(l,t') = A\sqrt{2l\pi^{1/2}} e^{-(1/2)(l\omega-k)^2} e^{i(\omega t'+\phi)} . \tag{8}$$

The cross-wavelet (eq. [5]) for these two signals becomes

$$\tilde{f}_c(l,t') = 2\sqrt{\pi}A_a A_m e^{i(\phi_a-\phi_m)} l e^{-k^2} \times e^{-(1/2)[(\omega_a^2+\omega_m^2)l^2-2kl(\omega_a+\omega_m)]} e^{(\omega_a-\omega_m)it'} . \tag{9}$$

Defining

$$A \equiv 2\sqrt{\pi}A_a A_m e^{-k^2} ,$$
$$\eta \equiv \omega_a^2 + \omega_m^2 ,$$
$$\gamma \equiv \omega_a + \omega_m ,$$
$$\beta \equiv \omega_a - \omega_m ,$$
$$\phi \equiv \phi_a - \phi_m ,$$

equation (9) then becomes

$$\tilde{f}_c(l,t') = Ale^{-(1/2)(\eta l^2-2k\gamma l)} e^{i(\beta t'+\phi)} , \tag{10}$$

which is easily interpreted. From this equation we note two important properties of this cross-wavelet: first, it has the form of a Gaussian in the dilation coordinate l, and second, it is sinusoidal in the translation coordinate t' with frequency given by the difference in the frequencies of the actual and the mock signal (i.e., the beat frequency). When these two frequencies are equal, the translation dependence is lost, and the cross-wavelet reduces to a Gaussian in the dilation coordinate. Figure 1*b* shows the cross-wavelet for two sinusoids oscillating with nearly the same frequency.

3.3. *Using the Cross-Wavelet Transform to Analyze Periodicity*

Motivated by the results from the previous section, we can develop an algorithm to find the period that best characterizes a signal, i.e., the characteristic timescale. Because we are dealing with real signals, noise will be present, and we explore the role of noise in §§ 4 and 5. In addition, the values of t and t' do not extend to infinity but over the range $t = a$

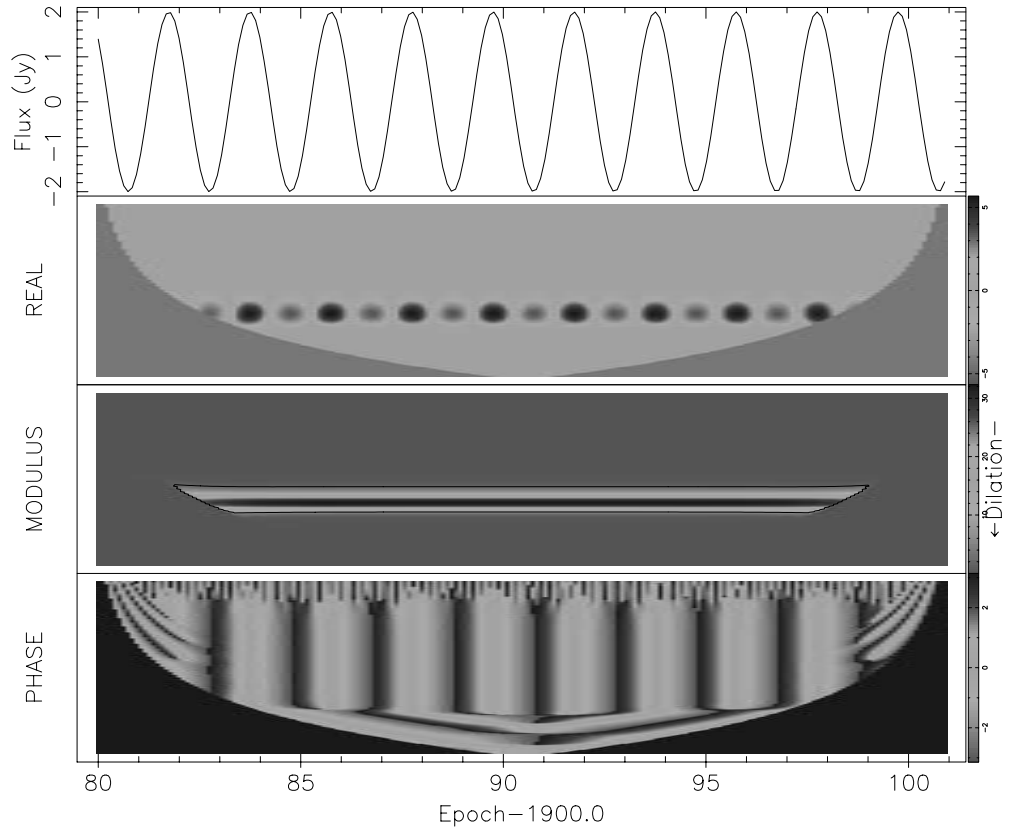


FIG. 1*a*

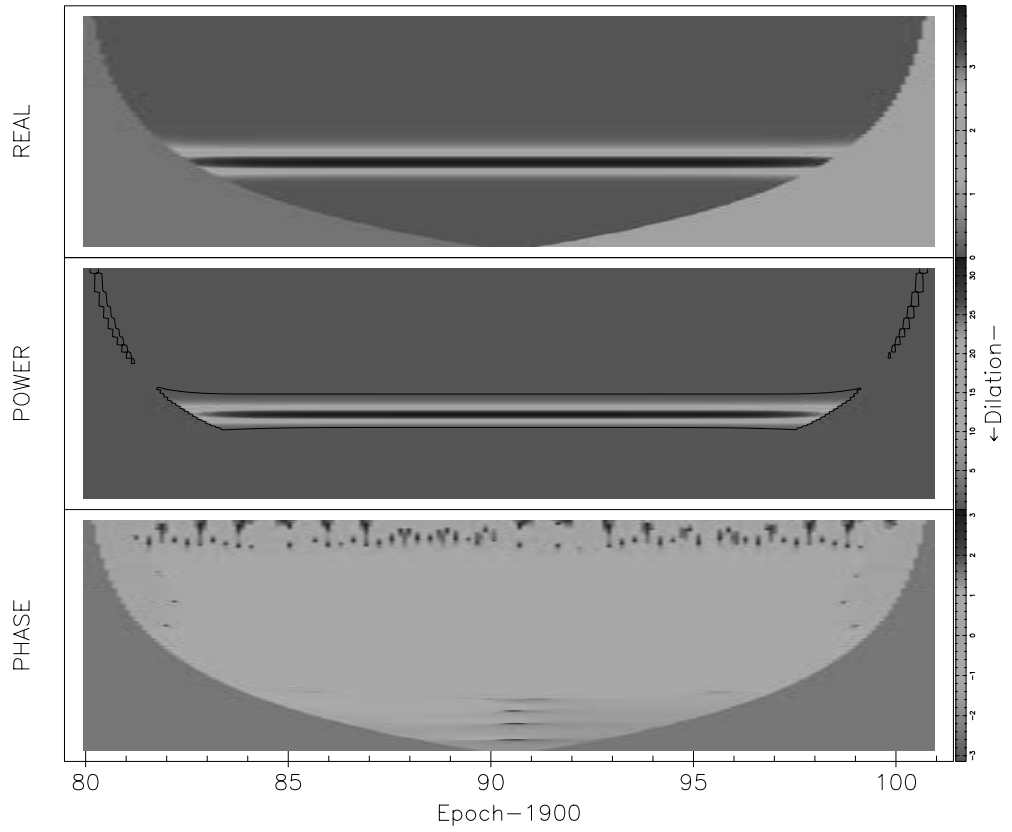


FIG. 1*b*

FIG. 1.—(*a*) Continuous wavelet transform for a sinusoid of period $\tau_a = 2.0$ yr. (*b*) Cross-wavelet transform for the sinusoid with another sinusoid of period $\tau_m = 2.059$ yr. The contours on both power (modulus) plots are for the 90% confidence level for correlated noise, assuming a lag-1 autocorrelation of $\alpha = 0.911362$. [*See the electronic edition of the Journal for a color version of this figure.*]

to $t = b$. Because of the finiteness of the range of t, the range of dilations becomes $l_{\min} < l < l_{\max}$. We can still use equation (8) as an approximation when our range of l and t' is such that the wavelets $\psi_{ll'}(t)$ contribute negligibly outside of $a < t < b$ and

$$\int_a^b e^{-\left\{[\omega-(k/l)]it\pm(1/2)|(t-t')/l|^2\right\}}dt \approx \int_{-\infty}^{\infty} e^{-\left\{[\omega-(k/l)]it\pm(1/2)|(t-t')/l|^2\right\}}dt\ . \quad (11)$$

Returning to equation (10), we define the modulus as

$$\left|\tilde{f}_c(l,t')\right|^2 = A^2 l^2 e^{-(\eta l^2 - 2k\gamma l)}\ . \quad (12)$$

Integrating over the region of wavelet space we mapped out, weighting by the scale, and approximating the integral over l, we arrive at

$$F_c(\tau_m) = \int_{l_{\min}}^{l_{\max}} \int_a^b \frac{\left|\tilde{f}_c(l,t')\right|^2}{l}\, dt'\, dl \approx A^2(b-a)\frac{k\gamma}{\eta}\sqrt{\frac{\pi}{\eta}}e^{(k^2\gamma^2)/\eta}\ . \quad (13)$$

We have empirically found that this function attains it maximum value at $\tau_a = 0.973\tau_m$ for a value of $k = 6$. This result is not surprising, since one would expect the power of the cross coefficients to reach their maximum when the periods for the two signals are almost equal. One can think of the mock signal as acting like a filter in wavelet space; however, the power of the mock coefficients, $|\tilde{f}_m|^2$, is slightly asymmetric about the peak (see eq. [8]). The weighted total power of the cross coefficients, F_c, does not attain its maximum exactly at $\tau_m = \tau_a$ because of this slight asymmetry.

To avoid confusion, one must remember that previously when the integration was over $[a, b]$ we integrated over the original coordinate t and, because the wavelets have compact support in t, we approximated the integral by taking the limits to be $[-\infty, \infty]$. Here, however, the integral is over the translation coordinate t', so we must restrict the limits to $[a, b]$. In addition, the approximation of the integral over l is valid so long as $\tilde{f}_c(l,t')/l$ does not peak in the dilation coordinate too close to $l_{\min}$ or $l_{\max}$. For our purposes, $l_{\min} = 2\delta t$ and $l_{\max} = N_{\rm data}\delta t/3$, where $N_{\rm data}$ is the number of data points and δt is the time spacing. Typical values of $b - a$ for the PR survey sources are roughly 20 yr, and we require at least $N_{\rm data} = 100$ data points for a reliable cross-wavelet analysis, which results in 0 yr $< l_{\min} \leq 0.4$ yr and $l_{\max} < 12$ yr. We search for periods within 0.5 yr $< \tau < (b-a)/4$ yr. We have inspected $|\tilde{f}_c|^2/l$ graphically to assure that the approximation is valid for periods $\tau_a \geq 0.7$ yr for all sources having more than 100 data points.

In practice, one must worry about edge effects since the time series is finite. Because the convolution of equation (2) introduces power into the wavelet coefficients $\tilde{f}$ from the discontinuity at the edges of the time series, there is a region where the wavelet coefficients will be contaminated from edge effects. This region is known as the *cone of influence*. The wavelet power associated with edge effects becomes negligible for translations t' farther than $\sqrt{2}l$ from the edge (Torrence & Compo 1998).

One more useful quantity is the point $\tilde{l}$ where $\tilde{f}_c(l,t')$ peaks in the dilation coordinate. This is given by

$$\tilde{l} = \frac{k(\omega_a+\omega_m) + \sqrt{(k^2+4)(\omega_a^2+\omega_m^2)+2k^2\omega_a\omega_m}}{2(\omega_a^2+\omega_m^2)}\ . \quad (14)$$

When $\omega_m = \omega_a$, this becomes

$$\tilde{l} = \frac{k+\sqrt{k^2+2}}{2\omega_a}\ , \quad (15)$$

or

$$\tau_a = \frac{4\pi\tilde{l}}{k+\sqrt{k^2+2}}\ , \quad \tau_a = \frac{2\pi}{\omega_a}\ . \quad (16)$$

This equation shows the relationship between a scale l and the corresponding Fourier period and can also be arrived at by inputting a sinusoid for $f(t)$ in equation (2). For clarification, we use the term "Fourier period" when referring to the period associated with a certain scale l and the term "analyzing period" or "mock period" when referring to the period τ_m associated with the mock signal.

4. SIGNIFICANCE TESTS

4.1. *Tests for the Continuous Transform*

Wavelet analysis has historically suffered from a lack of statistical significance tests. In Torrence & Compo (1998) an excellent discussion of statistical significance for the continuous wavelet transform is given and supported by Monte Carlo results, and we summarize the relevant points. When implementing the wavelet transform, one must use sums and discrete points rather than the theoretical treatment given earlier, and we switch to using these.

The model of correlated noise most likely to closely resemble the UMRAO data is the univariate lag-1 autoregressive [AR(1)] process (Hughes, Aller, & Aller 1992), given by

$$x_n = \alpha x_{n-1} + z_n\ , \quad (17)$$

where α is the assumed lag-1 autocorrelation and z_n is a random deviate taken from white noise (note that this is a "first-order" process). The normalized discrete Fourier power spectrum of this model is

$$P_j = \frac{1-\alpha^2}{1+\alpha^2-2\alpha\cos(2\pi\delta t/\tau_j)}\ , \quad (18)$$

where τ_j is the associated Fourier period (eq. [16]) of a scale l_j. If the time series of interest is an AR(1) process, then a slice in the modulus of the continuous coefficients, $|\tilde{f}(l,t')|^2$, along dilation at a constant translation (the *local wavelet power spectrum*), should have the form in equation (18). Note that a white-noise process is given by $\alpha = 0$.

Using the theoretical background spectrum given above, we can develop significance tests for the continuous transform. The background spectrum is the mean power spectrum expected for the assumed noise process (i.e., the "background" process), against which we wish to compare the actual signal. Physical processes that are the result of this background process will produce power spectra that are normally distributed about this mean background spectrum. Assuming that the values in our time series $f(t)$ are normally distributed, and because the

square of a normally distributed variable is χ^2 distributed with 1 degree of freedom, we expect the wavelet power $|\tilde{f}|^2$ to be χ^2 distributed with 2 degrees of freedom. The additional degree of freedom comes from the fact that the wavelet coefficients $\tilde{f}$ are complex for the Morlet wavelet. In addition, the expectation value for the wavelet power of a white-noise time series is just the variance σ^2; this expectation value provides a convenient normalization. Using this normalization, the distribution for the local wavelet power spectrum is

$$\frac{\left|\tilde{f}(l_j, t'_i)\right|^2}{\sigma^2} \Rightarrow P_j \frac{\chi^2_\nu}{\nu} , \tag{19}$$

where the double arrow means "is distributed as" and ν is the degrees of freedom, in this case 2. The indices on the scale l run from $j = 1, 2, \ldots, J$, where J is the number of scales, and the indices on the translation t' run from $i = 1, 2, \ldots, N_{\rm data}$.

We can also define the time-averaged wavelet power spectrum, or the *global wavelet spectrum*, as

$$\tilde{f}^2_G(l_j) = \frac{1}{N_j} \sum_{i=i_j}^{i'_j} \left|\tilde{f}(l_j, t'_i)\right|^2 , \tag{20}$$

where i_j and i'_j are the indices of the initial and final translations t'_i outside of the cone of influence at a given scale l_j, and N_j is the number of t'_i outside the cone of influence at that scale. It has been shown that the global wavelet spectrum provides an efficient estimation of the true power of a time series (Percival 1995). Averaging the wavelet power spectrum as in equation (20) increases the significance of the peaks, since the degrees of freedom are increased beyond what is used in the local wavelet power spectrum. However, because the coefficients are correlated in both time and scale, the degrees of freedom for the global wavelet spectrum are

$$\nu_j = 2\sqrt{1 + \left(\frac{N_j \delta t}{l_j \delta t_0}\right)^2} , \tag{21}$$

where δt_0 describes the decorrelation length in time. For the Morlet wavelet of $k = 6$, $\delta t_0 = 2.32$. The global wavelet spectrum of a sinusoid is shown in Figure 2.

Alternatively, we can smooth the wavelet spectrum in scale. We define the scale-averaged wavelet power as

$$\tilde{f}^2_L(t'_i) = \sum_{j=j_1}^{j_2} \frac{\left|\tilde{f}(l_j, t'_i)\right|^2}{l_j} . \tag{22}$$

The scale-averaged wavelet power can be interpreted as a time series of the average variance in the band $l_{j_1} \le l_j \le l_{j_2}$. This distribution can be modeled as

$$\frac{\tilde{f}^2_L(t'_i)}{\sigma^2} \Rightarrow \bar{P} \frac{\chi^2_{\nu_l}}{\nu_l} , \tag{23}$$

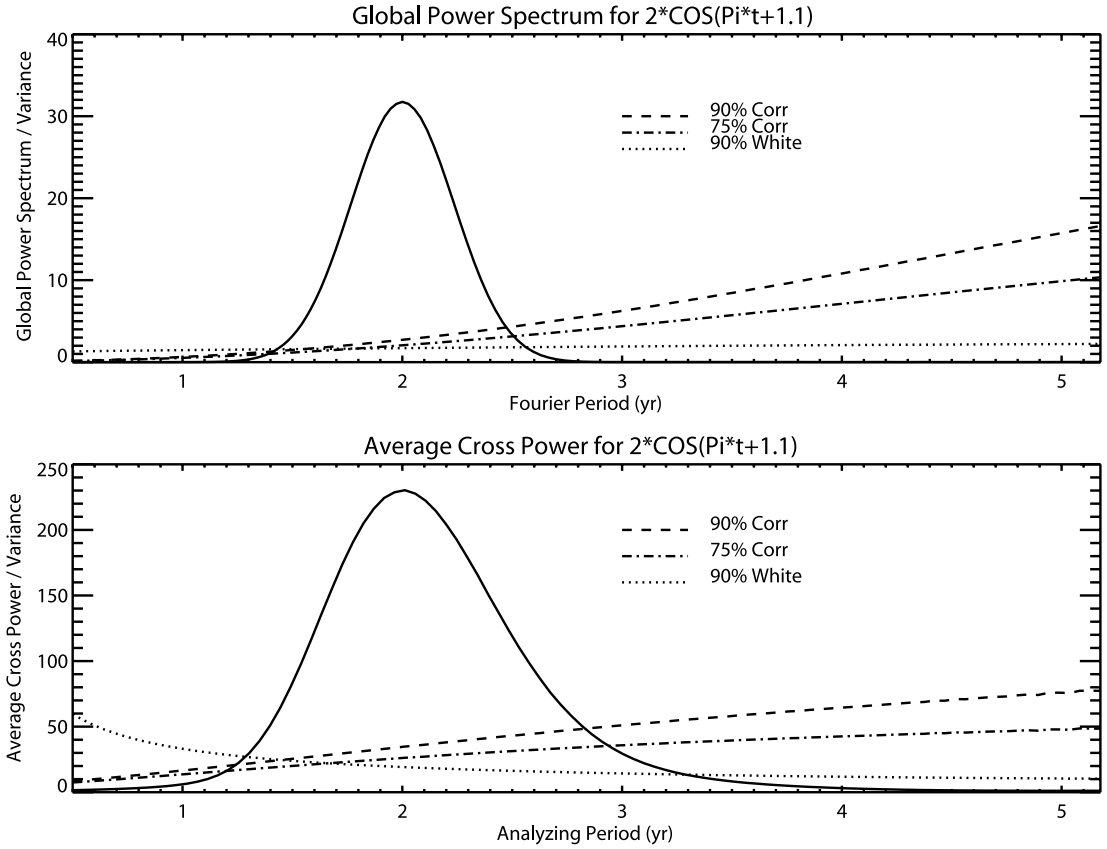


FIG. 2.—Global wavelet power spectrum $\tilde{f}^2_{\rm AG}(l_j)$ and the average cross power $\bar{F}_c(\tau_n)$ for a sinusoid of period $\tau_a = 2.0$ yr. Also shown are the confidence levels for white and correlated noise, assuming a lag-1 autocorrelation of $\alpha = 0.911362$.

where the scale-averaged theoretical spectrum $\bar{P}$ is

$$\bar{P} = \sum_{j=j_1}^{j_2} \frac{P_j}{l_j} \ . \tag{24}$$

The degrees of freedom ν_l in equation (24) are modeled as

$$\nu_l = \frac{2N_l L_{\text{avg}}}{L_{\text{mid}}} \sqrt{1 + \left(\frac{N_l \delta j}{\delta j_0}\right)^2} \ , \tag{25}$$

where

$$L_{\text{avg}} = \left(\sum_{j=j_1}^{j_2} \frac{1}{l_j} \right)^{-1} \ ,$$
$$L_{\text{mid}} = l_{\min} 2^{0.5(j_1+j_2)\delta j} \ ,$$
$$l_j = l_{\min} 2^{(j-1)\delta j} \ , \quad j = 1, \ 2, \ \ldots, \ J \ ,$$

N_l is the number of dilations averaged over, and δj_0 is the decorrelation distance in scale. For the Morlet wavelet of $k = 6$, $\delta j_0 = 0.60$. The δj describes how the dilations l_j are constructed; it is common to construct them as fractional powers of 2 since it allows more emphasis on the smaller scales. The factor $L_{\text{avg}}/L_{\text{mid}}$ corrects for the loss of degrees of freedom from dividing the wavelet power spectrum by scale in equation (22).

4.2. *Tests for the Cross Transform*

Using the results of Torrence & Compo (1998) from the previous section, we can derive significance tests for the cross-wavelet transform. The power of the cross-wavelet $\tilde{f}_c$ can be written as

$$\left|\tilde{f}_c(l_j, t_i')\right|^2 = \left|\tilde{f}_a(l_j, t_i')\tilde{f}_m^*(l_j, t_i')\right|^2 = \left|\tilde{f}_a(l_j, t_i')\right|^2 \left|\tilde{f}_m(l_j, t_i')\right|^2 \tag{26}$$

and is distributed as

$$\frac{\left|\tilde{f}_a(l_j, t_i')\right|^2 \left|\tilde{f}_m(l_j, t_i')\right|^2}{\sigma^2} \Rightarrow P_j \left|\tilde{f}_m(l_j, t_i')\right|^2 \frac{\chi_\nu^2}{\nu} \ , \tag{27}$$

where the degrees of freedom ν is 2. We can also define the cross-wavelet global power spectrum,

$$\tilde{f}_{\text{CG}}^2(l_j) = \frac{1}{N_j} \sum_{i=i_j}^{i_j'} \left|\tilde{f}_c(l_j, t_i')\right|^2 \ . \tag{28}$$

Noting that the power of the continuous coefficients for the type of mock signal given in equation (7) is independent of the translation t', the time-averaged form of equation (13), F_c, then becomes

$$\bar{F}_c(\tau_m) = \sum_{j=1}^{J} \frac{\tilde{f}_{\text{CG}}^2(l_j)}{l_j} = \sum_{j=1}^{J} \frac{\tilde{f}_{\text{AG}}^2(l_j)\left|\tilde{f}_m(l_j)\right|^2}{l_j} \ , \tag{29}$$

where $\tilde{f}_{\text{AG}}^2(l_j)$ is the global wavelet power spectrum for the actual signal $f_a(t_i)$. This distribution can be modeled as

$$\bar{F}_c(\tau_m) \Rightarrow \sum_{j=1}^{J} \frac{P_j \left|\tilde{f}_m(l_j)\right|^2}{l_j} \left(\frac{\chi_{\nu_j'}^2}{\nu_j'}\right) \ , \tag{30}$$

where the degrees of freedom ν_j' are modeled as

$$\nu_j' = \nu_j + \nu_l \ , \tag{31}$$

for ν_j and ν_l given in the previous section. This allows us to smooth the wavelet power in both time and scale, thus increasing the degrees of freedom, and to receive information of the characteristic timescale(s) of our time series from the mock coefficients $\tilde{f}_m$ rather than from the global wavelet spectrum. As mentioned in § 3.3, equation (29) allows us to interpret the cross-wavelet of a time series and an analyzing signal as a filter in wavelet space, where the coefficients of the continuous transform for the analyzing signal filter the global wavelet spectrum of our time series, $\tilde{f}_{\text{AG}}^2$. Averaging the cross transform in scale then allows us to find the analyzing signal with which the time series is best correlated over the entire range of time and scale. A plot of $\bar{F}_c$ for a sinusoid can be seen in Figure 2.

The results of this section are valid only when the cross-wavelet consists of one source that has an assumed background spectrum that is χ^2 distributed. If one is crossing two sources, $f_1(t)$ and $f_2(t)$, that have assumed background spectra, P_1 and P_2, that are χ^2 distributed, then the cross-wavelet is distributed as

$$\frac{\left|\tilde{f}_1(l, t)\tilde{f}_2^*(l, t)\right|}{\sigma_1 \sigma_2} \Rightarrow \frac{Z_\nu(p)}{\nu} \sqrt{P_1 P_2} \ , \tag{32}$$

where σ_1 and σ_2 are the respective standard deviations, the degrees of freedom ν is 2 for complex wavelets, and $Z_\nu(p)$ is the confidence level for a given probability p for the square root of the product of two χ^2 distributions (Torrence & Compo 1998). One can find the confidence level Z_ν by inverting the integral $p = \int_0^{Z_\nu} f_\nu(z)\, dz$. The probability distribution is given by

$$f_\nu(z) = \frac{2^{2-\nu}}{\Gamma^2(\nu/2)} z^{\nu-1} K_0(z) \ , \tag{33}$$

where z is the random variable, Γ is the Gamma function, and $K_0(z)$ is the modified Bessel function of order zero.

5. ALGORITHM FOR IMPLEMENTING THE CROSS TRANSFORM TO ANALYZE QUASI-PERIODIC BEHAVIOR AND SIMULATIONS

5.1. *Algorithm for Analysis of Quasi-periodic Behavior*

When using real data, we have no a priori knowledge, if any, of the periodicity for the particular signal of interest and require an algorithm that will allow us to find it. The results of §§ 3.3 and 4 will serve as a guide in developing this. First, we subtract the mean from the signal and perform the continuous wavelet transform given by equation (1), only multiplying by a factor of $(\delta t)^{1/2}$ to allow proper normalization and replacing the integral with a sum. Then, we divide the continuous coefficients by the standard deviation of the time series to assure that the expectation value of $|\tilde{f}|^2$ for white noise is unity and cross them with the coefficients for a number of mock (analyzing) signals, each of which has a period $\tau_n = \tau_{n-1} + \delta\tau$. For each of these, we average over the relevant region in wavelet space as in equation (29) and look for extrema. The extrema of $\bar{F}_c(\tau_n)$ then correspond to characteristic timescales related by $\tau_a = 0.973\tilde{\tau}_n$, where $\tilde{\tau}_n$ is

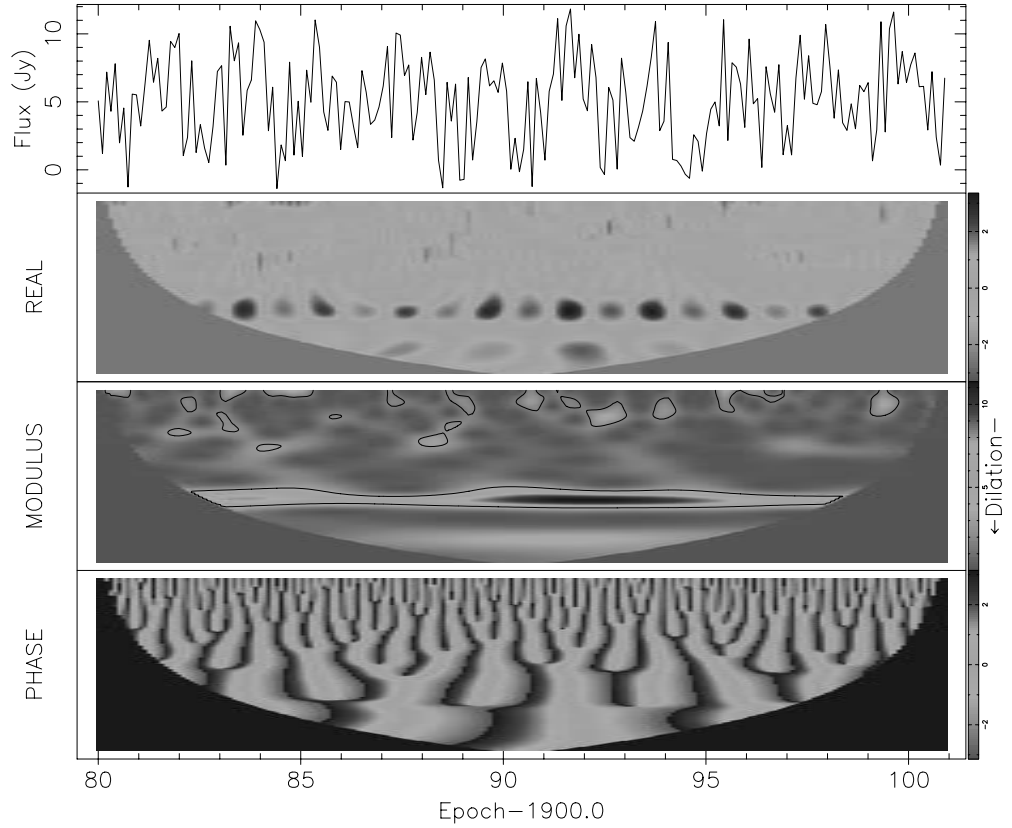


FIG. 3*a*

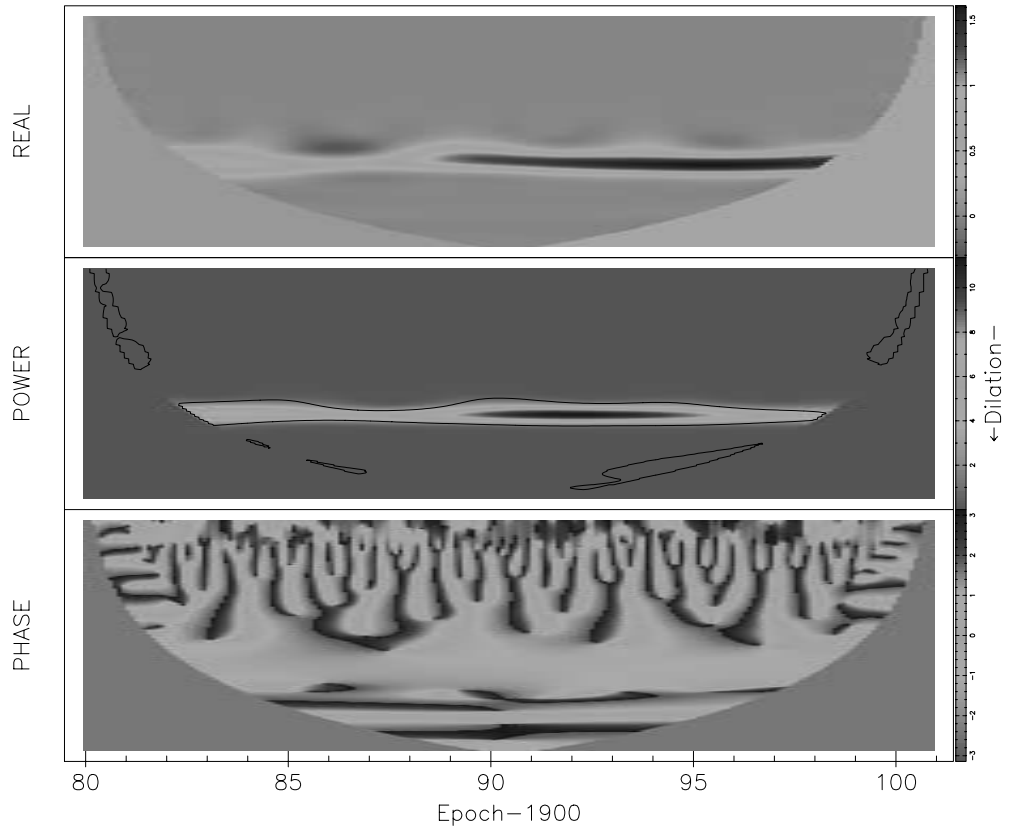


FIG. 3*b*

FIG. 3.—(*a*) Continuous wavelet transform for a sinusoid of period $\tau_a = 2.0$ yr with white noise added, S/N = 0.2. (*b*) Cross-wavelet for the sinusoid of (*a*). The contours on both power plots are for the 90% confidence level for correlated noise, assuming a lag-1 autocorrelation of $\alpha = 0.283620$. [*See the electronic edition of the Journal for a color version of this figure.*]

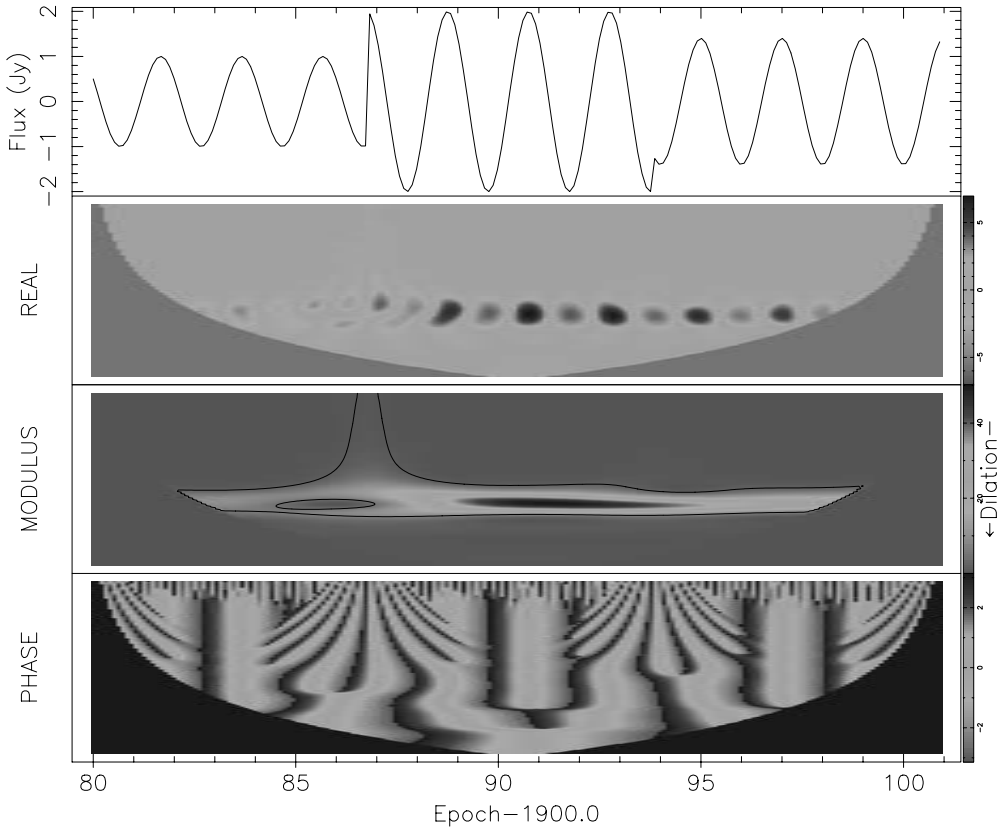


FIG. 4*a*

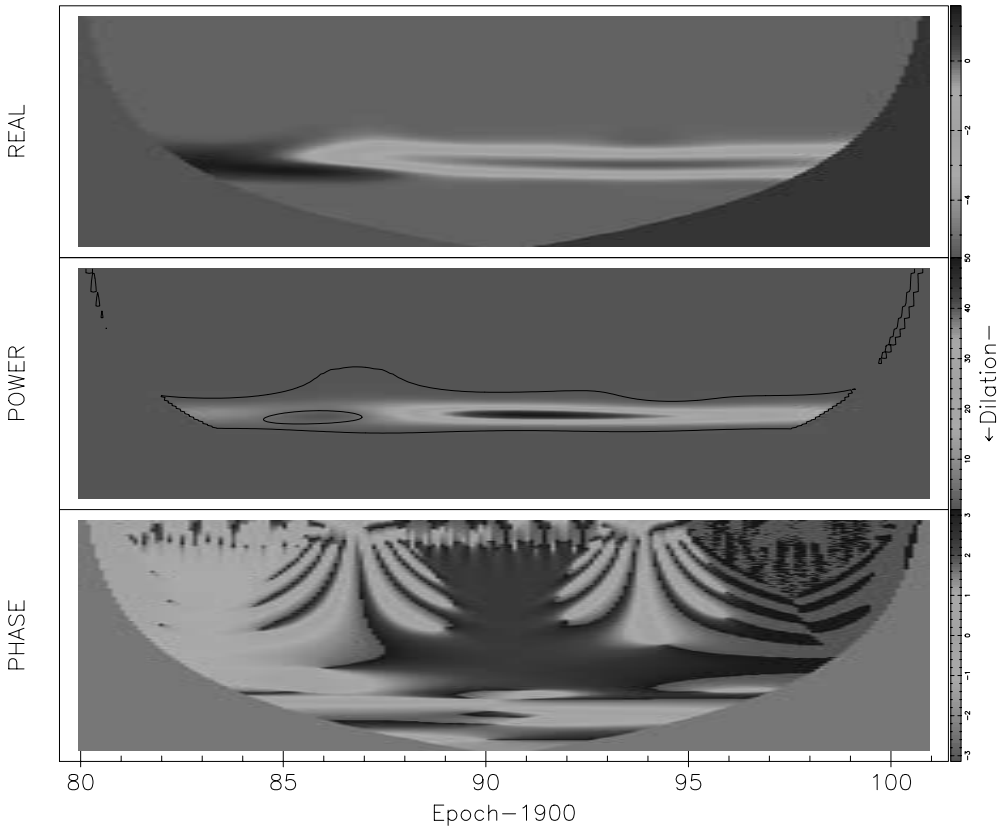


FIG. 4*b*

FIG. 4.—(*a*) Continuous wavelet transform for a sinusoid of period $\tau_a = 2.0$ yr and varying amplitude and phase. (*b*) Cross-wavelet transform for the sinusoid of (*a*). The contours on both power plots are for the 90% confidence level for correlated noise, assuming a lag-1 autocorrelation of $\alpha = 0.894581$. [*See the electronic edition of the Journal for a color version of this figure.*]

the period of the mock signal corresponding to the extremum.

The nth mock signal is given by

$$f_n(t) = A_n \cos\left(\frac{2\pi}{\tau_n} t + \phi_n\right) , \tag{34}$$

where we use the subscript n instead of m on the parameters to emphasize that they are for the nth mock signal. We choose a value of A_n such that the global wavelet spectrum of the analyzing signal is normalized so that its maximum value is unity. This provides a convenient normalization among the analyzing signals, assuring that they all have the same power. In this analysis, 100 mock signals are used to analyze the actual time series, resulting in a step size of $\delta\tau \sim 0.045$ for most sources (this varies slightly because not all of the sources have the same time window). We set ϕ_n equal to zero, since $|\tilde{f}_c|^2$ is independent of the phase difference between the signals. Many of the signals analyzed in this paper have typical values for the time range on the order of $a = 80$ yr and $b = 101$ yr, which arise from using the year 1900 as a baseline. The dilation values are chosen such that $2\delta t \text{ yr} < l < N_{\text{data}}\delta t/3$ yr, which allows us to be conservative when omitting edge effects and to admit the approximations used in equations (8) and (13).

When plotting the coefficients, those that fell within the cone of influence at any given dilation were set to a constant value, thus masking the edge effects. Values of l_j are shown logarithmically, so as to allow more sensitivity in the dilation region corresponding to shorter mock periods. It is helpful to examine the global wavelet spectrum of the time series (eq. [20]) and to compare with the cross-wavelet results, so we include it in our analysis. We assume a background spectrum P_j of the form AR(1) (eq. [18]) and estimate the lag-1 autocorrelation coefficient by calculating the lag-1 and lag-2 autocorrelations, α_1 and α_2. The lag-1 autocorrelation coefficient is then estimated as $\alpha = (\alpha_1 + \sqrt{\alpha_2})/2$. The background spectrum P_j then allows us to compute confidence levels using the results of § 4. We plot contours on the continuous and cross-wavelet transforms corresponding to the 90% confidence level for an AR(1) process. We also plot 90% and 75% correlated noise confidence levels on the plots of the global wavelet spectrum f^2_{AG} and the averaged cross-wavelet power $\bar{F}_c(\tau_n)$, as well as 90% confidence levels for white noise ($P_j = 1$). It should be noted that by confidence level, we mean that this given percentage of assumed background (i.e., noise) processes will produce behavior less than what is seen in the wavelet transforms. For the time series analyzed here, the 90% confidence levels for correlated noise mark where 90% of AR(1) processes will produce values *less* than the 90% values, and likewise for the 75% confidence levels and the 90% confidence levels for white noise.

To satisfy the admissibility condition (4), we choose a value of $k = 6$. In reality, equation (4) is not formally satisfied for the Morlet wavelet of equation (1). However, if $k \geq 5$, the admissibility condition is satisfied to within the accuracy of computer algorithms using single-precision arithmetic.

5.2. *Simulations*

To test our technique, we ran several simulations. First, to investigate the ability of our technique to detect a purely periodic signal in the presence of noise, we used a signal of the form

$$f_a(t) = 2\sin(\pi t + 1.1) + Nn(t) , \tag{35}$$

where N is an amplitude factor and $n(t)$ a noise function that generates white noise. We show the continuous and cross transforms for $N = 10$ in Figure 3. The cross-wavelet plot is that for a mock signal of period $\tau_n = 2.059$ yr. Plots of the global wavelet spectrum and $\bar{F}_c$ for this simulation are shown in the top two panels of Figure 5. As can be seen in these two panels, the period is easily recovered using the technique with noise of amplitude 5 times that of the amplitude of the sinusoid (S/N = 0.2). Because S/N values as low as S/N = 0.2 are never realized, our technique is valid for the time series studied here.

In addition, we also applied the algorithm to a sinusoid that changes amplitude and phase over the time window. The transforms are shown in Figure 4, and the power spectra in the bottom two panels of Figure 5. A change in amplitude affects the amplitude of the wavelet coefficients, as would be expected. The effects of a discontinuous change in the phase ϕ_a can be seen as disturbing the structure of the

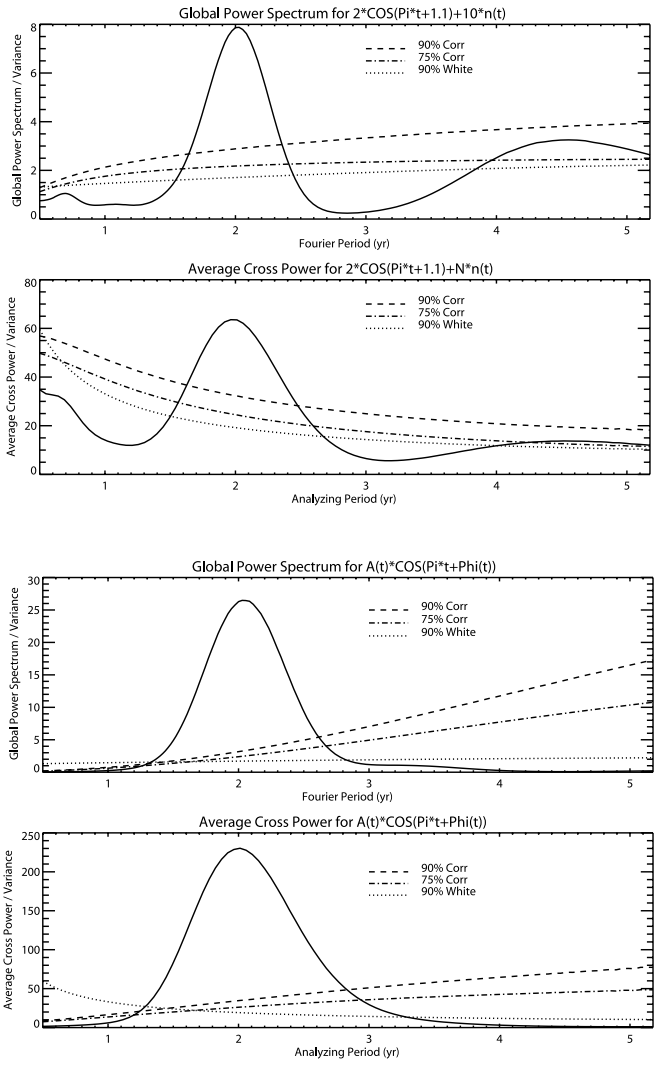


FIG. 5.—Global power spectrum $\tilde{f}^2_{\text{AG}}(l_j)$ and average cross power $\bar{F}_c(\tau_n)$ for the sinusoids of Fig. 3 (*top two panels*) and Fig. 4 (*bottom two panels*). Confidence levels for correlated and white noise are shown.

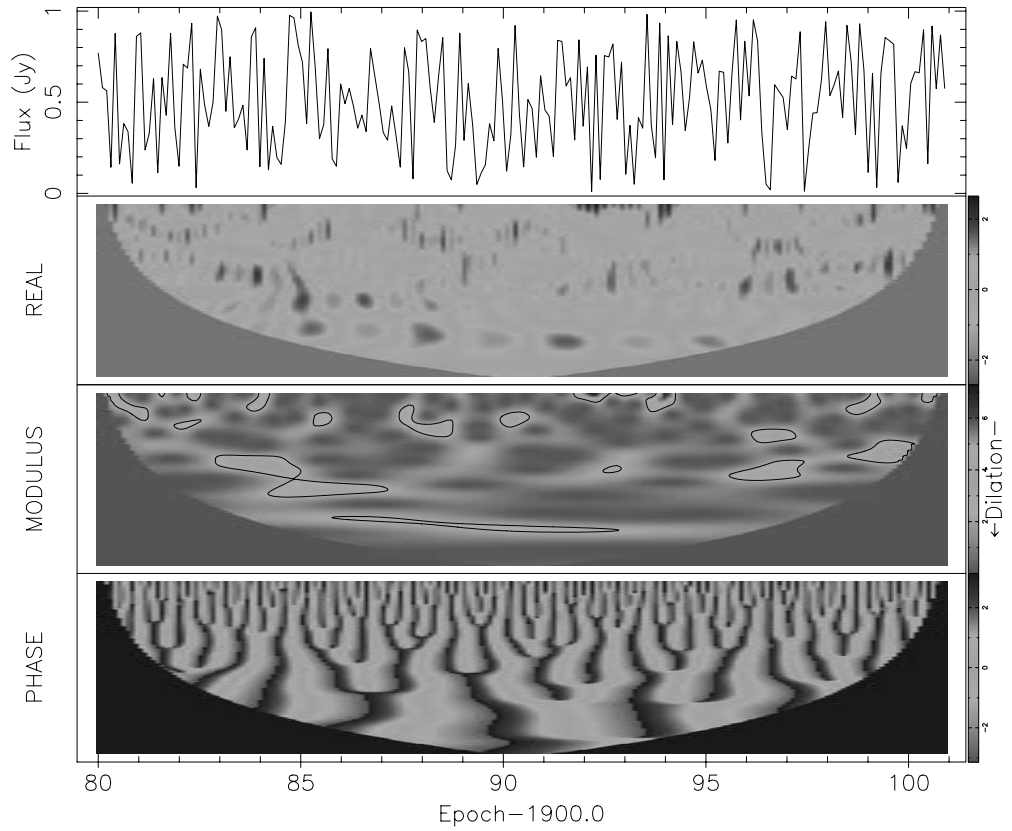


FIG. 6*a*

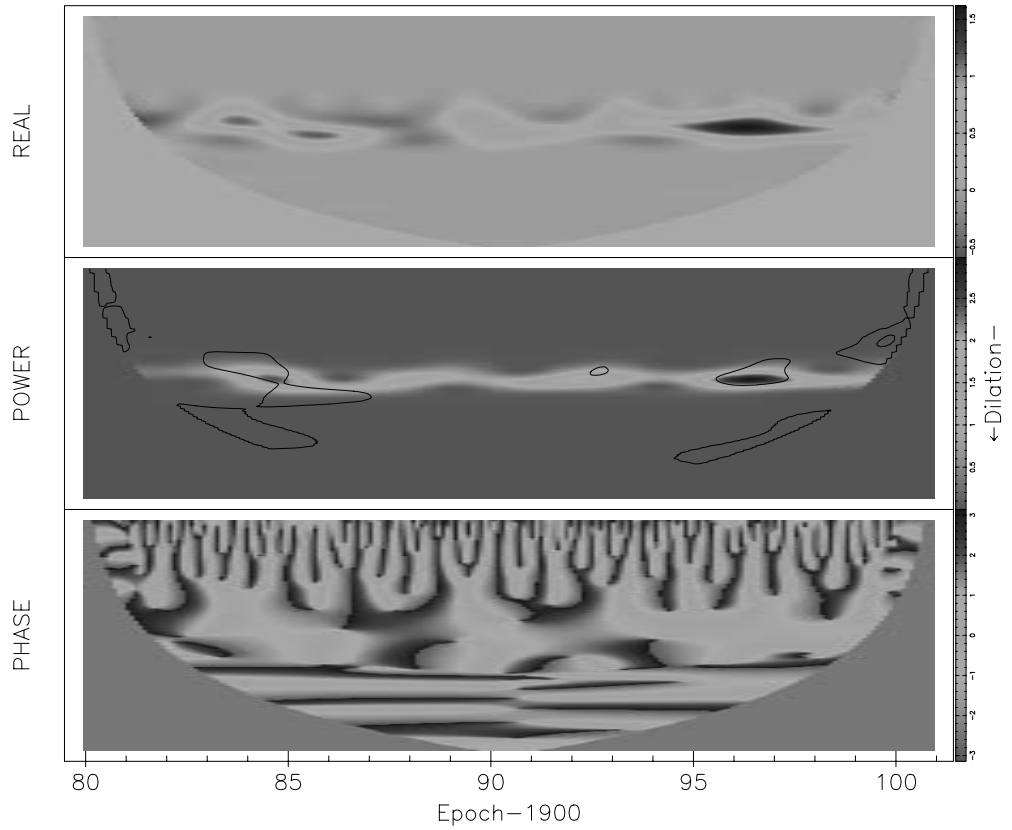


FIG. 6*b*

FIG. 6.—(*a*) Continuous wavelet transform for a Gaussian white-noise signal. White noise is easily recognizable by its erratic and complex structure in wavelet space, particularly at small dilations. (*b*) Cross-wavelet transform for the Gaussian white-noise signal, corresponding to an analyzing signal of period $\tau_n = 0.736$ yr. The contours on both power plots are for the 90% confidence level for white noise. [*See the electronic edition of the Journal for a color version of this figure.*]

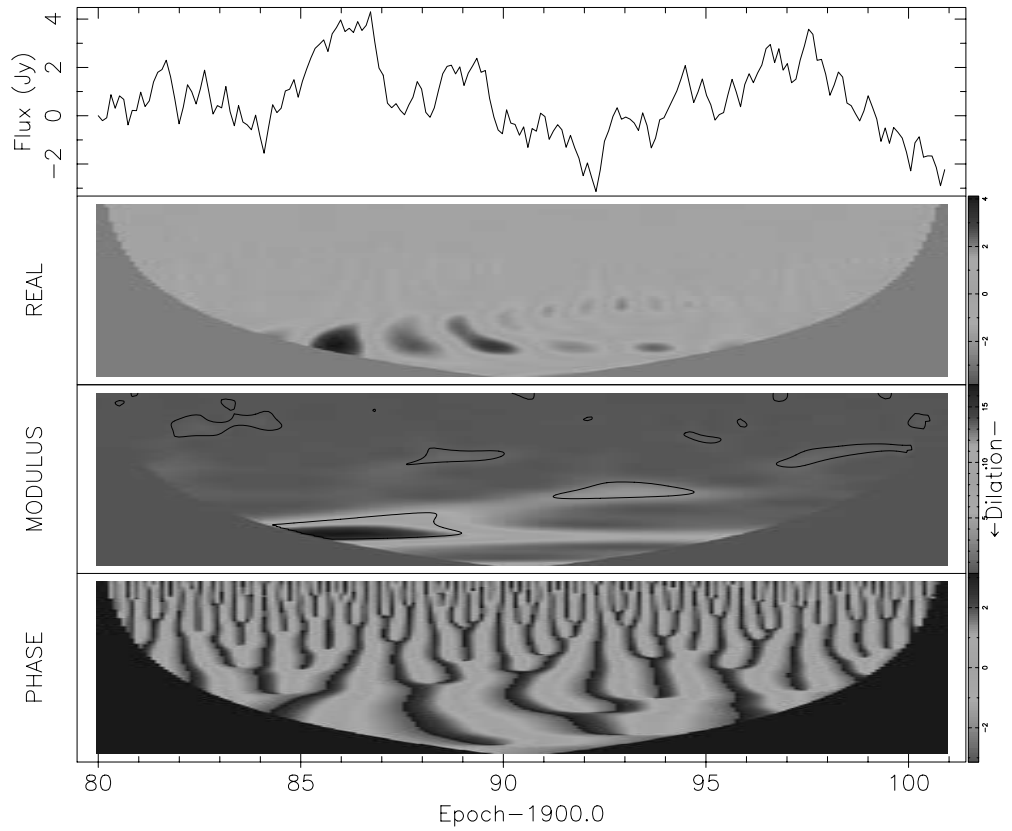


FIG. 7*a*

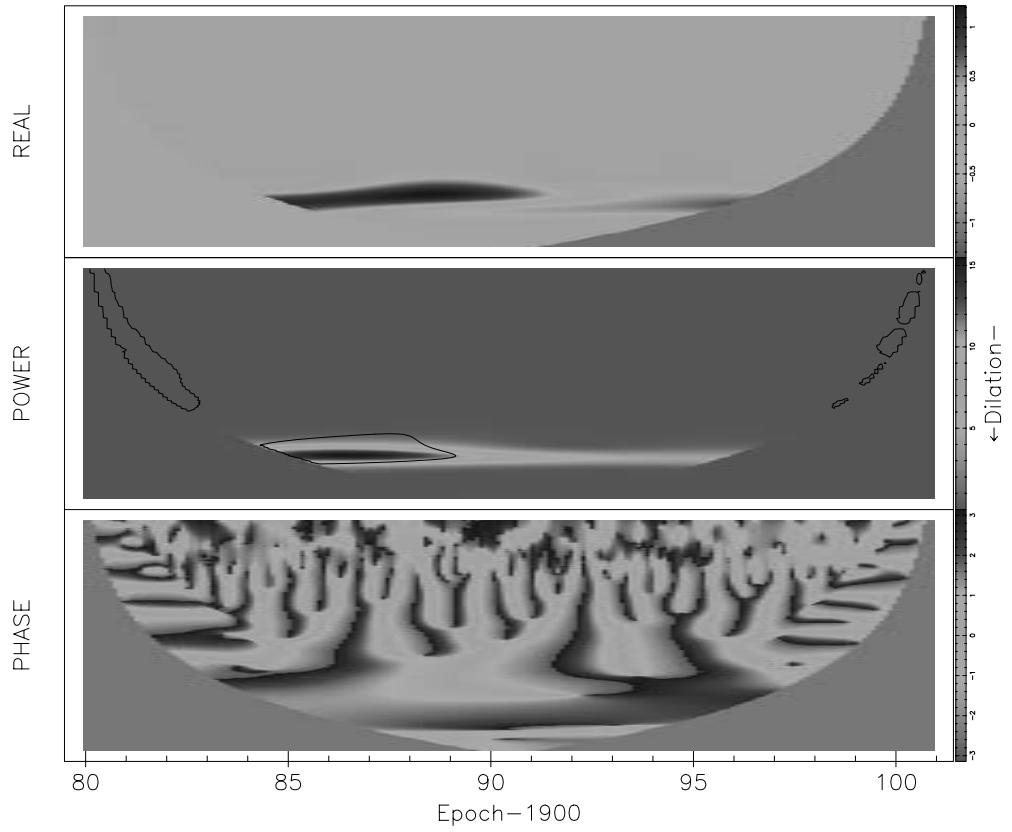


FIG. 7*b*

FIG. 7.—(*a*) Continuous wavelet transform for a correlated noise signal of the form AR(1), with lag-1 autocorrelation coefficient $\alpha = 0.9$. (*b*) Cross-wavelet transform for the correlated noise signal. The signal is crossed with a mock signal of period $\tau_n = 3.901$ yr. The contours on both power plots are for the 90% confidence level for an AR(1) process of $\alpha = 0.9$. [*See the electronic edition of the Journal for a color version of this figure.*]

transforms in these regions. The technique gives a characteristic period of 2.0 yr, showing that a sudden change in the phase of a signal does not affect the technique.

In practice, we are using this technique to investigate quasi-periodic behavior and to give a characteristic timescale for a time series, rather than attempting to recover a periodic signal buried beneath noise (although this certainly can be done). To illustrate our technique in the case of pure noise, we applied the cross-wavelet technique to Gaussian white noise and correlated noise. The wavelet transforms for a white-noise signal are shown in Figure 6. As can be seen, temporary quasi-periodic structure can arise for white noise; however, the signal is clearly distinguished from more coherent signals by the complex structure throughout the plot, particularly in the low-dilation (high-frequency) region. Plots of the global wavelet power spectrum and the averaged cross power $\bar{F}_c$ are shown in the top two panels of Figure 8. Although there are distinct peaks in the global spectrum at small scales, the average power of the cross-wavelet, $\bar{F}_c$, does not show distinct peaks at these scales. We interpret this as being the result of smoothing in scale as well as time when calculating $\bar{F}_c$; the global wavelet spectrum is averaged in time for a given dilation l_j and can result in peaks even in the case of nonstationary power, as is seen in the continuous plot for white noise. However, by crossing with an analyzing signal and averaging in dilation, we can smooth out spurious extrema, as is seen in the plot of $\bar{F}_c$.

To illustrate the technique for correlated noise, we used a test signal of the type AR(1) with lag-1 autocorrelation $\alpha = 0.9$. Many of the PR sources had lag-1 autocorrelations of $\alpha \sim 0.9$, and we found it helpful to simulate an AR(1) process of α similar to what we infer for the data. Figure 7 shows the transforms for this signal. As expected, there is more activity at larger scales (lower frequencies). Coherent activity does appear in the case of this type of correlated noise; however, the power is not stationary and cannot be characterized by a particular scale. The global power spectrum and $\bar{F}_c$ can be seen in the bottom two panels of Figure 8. Peaks appear at similar periods for both; however, the plot of $\bar{F}_c$ shows that the peaks are less significant than those seen in the global power spectrum. The reason for this can be seen in the continuous plot; the power appears to split into two timescales around $t' = 90$. When we cross the continuous transform with our analyzing signal transform and average over both translation and dilation, we see that the timescale of $\sim$3.8 yr is not as significant as it appears in the global wavelet spectrum.

We can see from the simulations, as well as from the results of applying the transforms to the PR sources, that the average cross power, $\bar{F}_c(\tau_n)$, places more emphasis on the smaller scales and periods than the global power spectrum. This is to be expected, since the amplitude of the global power spectrum for the time series of interest, $\tilde{f}^2_{\rm AG}(l_j)$, has a dependence on the scale l_j (see eq. [8]). If we do not normalize the global power spectrum of the mock signal, $|\tilde{f}_m|^2$, such that its maximum value is unity for all periods τ_n, then the amplitude of $|\tilde{f}_m|^2$ will also have a scale dependence. This would result in the amplitude of $\bar{F}_c$ being dependent on the scale l_j as well (note that $\bar{F}_c$ would not be dependent on l_j^2 because we divide by the scale in eq. [29]). However, normalizing the mock power spectrum $|\tilde{f}_m|^2$ so that its maximum value is unity removes the scale dependence in $|\tilde{f}_m|^2$ and thus in $\bar{F}_c$.

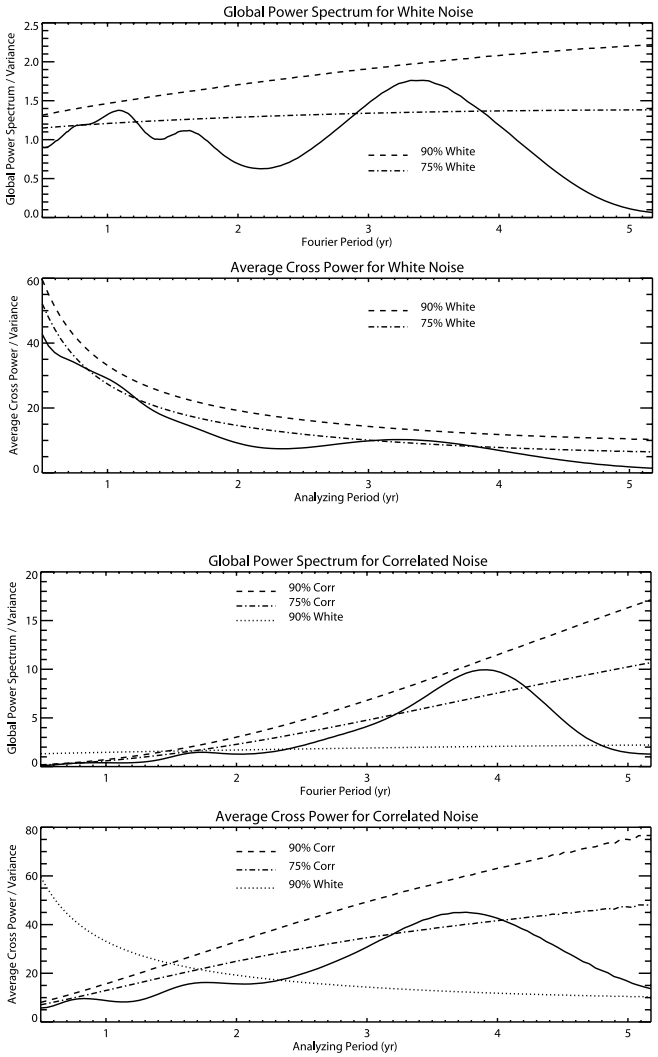


FIG. 8.—Global power spectrum $\tilde{f}^2_{\rm AG}(l_j)$ and average cross power $\bar{F}_c(\tau_n)$ for the white-noise signal of Fig. 6 (*top two panels*) and the correlated noise signal of Fig. 7 (*bottom two panels*). Confidence levels for correlated and white noise are shown.

In addition, we applied the cross-wavelet transform technique to the BL Lac objects OJ 287 and AO 0235+164, since previous analysis has shown evidence for periodicity in these sources. For OJ 287 the technique detected a characteristic timescale of $\sim$1.6 yr, with a shorter timescale of $\sim$1.1 yr, confirming results found earlier by Hughes et al. (1998). The cross-wavelet analysis also confirmed earlier results for AO 0235+164, giving timescales of $\sim$1.9 and $\sim$3.3 yr, which is in good agreement with the 3.61 yr found by Roy et al. (2000) using a Lomb-Scargle periodogram. We were not able to confirm the longer periods found by Roy et al. (2000), since they fell outside of our condition of at least four cycles in the time window.

6. THE DATA ANALYSIS

The results of using the algorithm described in § 5.1 to search UMRAO data on the PR survey sources are given in Table 1. Observations that we considered to have insufficient data to give a reliable analysis of quasi-periodicity (about half) are denoted by "D." Such observations were

TABLE 1

CHARACTERISTIC PERIODS FOUND USING THE CROSS-WAVELET ALGORITHM ON THE PEARSON-READHEAD VLBI SURVEY SOURCES

		4.8 GHz		8.0 GHz		14.5 GHz	
SOURCE	OPTICAL CLASS	Period	Data	Period	Data	Period	Data
0016+731	Q	...	218	...	170	3.3	249
3C 20	G	D		D		D	
0108+388	G	D		...	125	D	
DA 55	Q	...	566	...	811	2.3	674
0153+744	Q	D		D		D	
0212+735	Q	...	228	...	244	4.1	263
3C 66B	G	D		D		D	
3C 83.1	G	D		D		D	
3C 84	G	...	636	...	1617	...	872
0404+768	G	D		D		D	
3C 147	Q	...	141	...	173	...	134
3C 153	G	D		D		D	
OI 147	G	D		D		D	
OI 318	Q	...	134	1.0	133	0.7	124
3C 179	Q	...	136	1.0	125	2.2	134
0804+499	Q	2.7, 1.8, 1.2	193	1.1	196	1.1	177
3C 196	Q	D		D		D	
0814+425	BL	...	177	...	462	...	282
0831+557	G	D		D		D	
0836+710	Q	2.6	222	1.4	166	...	271
0850+581	Q	D		D		D	
0859+470	Q	D		D		D	
3C 216	Q	...	189	...	228	...	194
3C 219	G	D		D		D	
4C 39.25	Q	...	554	...	1282	...	815
4C 20.24	Q	D		3.6	141	3.7	104
M82	G	D		D		D	
0954+556	Q	D		...	124	...	103
0954+658	BL	...	167	...	150	...	221
3C 236	G	D		D		D	
1031+567	G	D		D		D	
3C 268.1	G	D		D		D	
3C 280	G	D		D		D	
4C 66.22	G	1.3	168	...	176	0.9	147
3C 295	G	D		D		D	
3C 309.1	Q	D		D		D	
3C 330	G	D		D		D	
4C 41.43	Q	D		D		D	
1633+382	Q	...	244	...	432	...	315
3C 343	Q	D		D		D	
1637+574	Q	D		D		D	
3C 345	Q	...	851	...	1529	5.1	927
1642+690	Q	...	167	...	331	4.9	278
Mrk 501	BL	...	230	...	525	...	302
1739+522	Q	1.4	248	1.4	348	1.2	383
1749+701	BL	...	217	...	357	...	256
1803+784	BL	2.0, 3.9	272	2.0	300	...	419
3C 371	BL	...	220	...	451	...	307
1823+568	BL	3.3	135	...	241	3.3	275
3C 380	Q	D		D		D	
3C 388	G	D		D		D	
3C 390.3	G	D		3.4, 2.4	150	...	154
1928+738	Q	...	315	...	356	...	469
3C 401	G	D		D		D	
OV 591	Q	D		D		D	
OW 673	Q	D		D		D	
3C 438	G	D		D		D	
BL Lac	BL	1.4	856	3.7	1441	3.5, 1.6, 0.7	1243
2229+391	G	D		D		D	
3C 452	G	D		D		D	
2351+456	Q	...	148	D		3.8	167
DA 611	G	D		D		D	

NOTES.—All periods are in years. "D" signifies insufficient data; an ellipsis signifies no detected quasi-periodicity. The number of data points is given only for those sources with sufficient data. If two timescales are given, the more prominent one is listed first.

TABLE 2
QUASI-PERIODICITY STATISTICS

Type (1)	Sources (2)	Time Series (3)	Mean Timescale (yr) (4)	Standard Deviation (yr) (5)	Q/S (6)	Q_t/T (7)	M/Q (8)
Quasars	18	51	2.3	1.4	0.67	0.43	0.5
Galaxies	4	10	2.0	1.1	0.5	0.4	0.5
BL Lac objects	8	24	2.5	1.1	0.38	0.42	1.0
All types	30	85	2.4	1.3	0.57	0.42	0.59

NOTES.—Q/S is the ratio of sources exhibiting quasi-periodicity in at least one observing frequency to the total number of sources, Q_t/T is the ratio of the total number of timescales to the total number of time series, and M/Q is the ratio of sources that showed quasi-periodicity in more than one observing frequency to the total number of quasi-periodic sources.

excluded because we required at least 100 data points for a given time series, since we assumed that 100 points are needed to adequately define its character. When analyzing the light curves, we used the entire time window, which varied between observing frequencies and sources. Since we are using a finite step size $\delta\tau \sim 0.045$ yr, we do not expect to use an analyzing signal with period $\tau_n = \tau_a$, but rather with period $\tau_n \approx \tau_a$. However, because we are analyzing quasi-periodic behavior we do not expect the sources to have a well-defined period (i.e., a spike in Fourier space), but rather a characteristic timescale. The error resulting from the finite step size of 0.045 yr is irrelevant in this context, since there is no sense found in assigning an extremely precise value for a quasi-periodic source. We record timescales only at or above the 90% confidence level.

Many of the sources that exhibited quasi-periodic variations had characteristic timescales between 1 and 4 yr, with an average timescale for all quasi-periodic sources of 2.4 yr and a standard deviation of 1.3 yr. This, of course, is to be expected since our observing interval is around 20 yr and we are interested only in variations with at least four possible repetitions across the interval. Table 2 shows statistics with

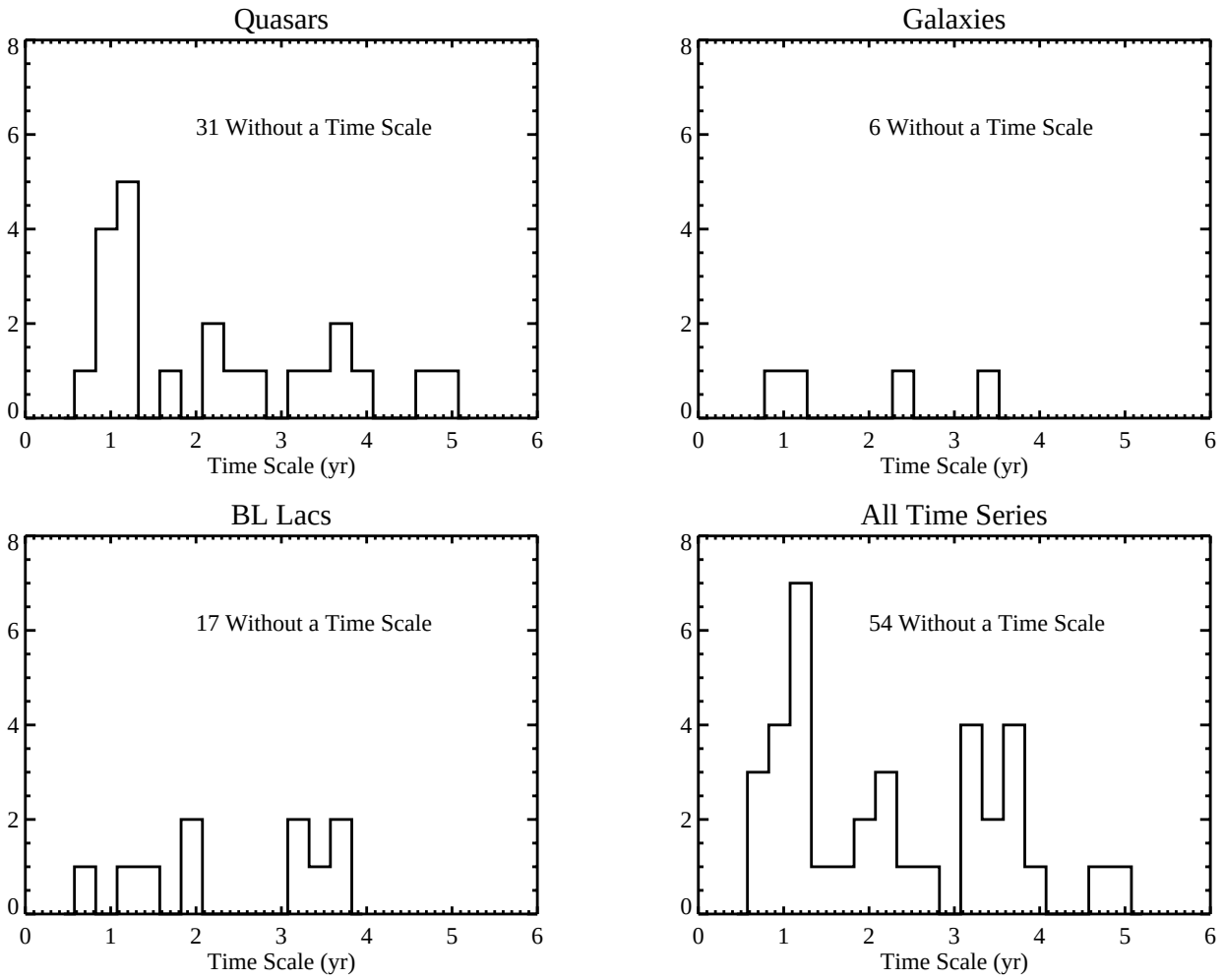


FIG. 9.—Histograms for the quasi-periodicity statistics. Timescales are binned every 0.25 yr.

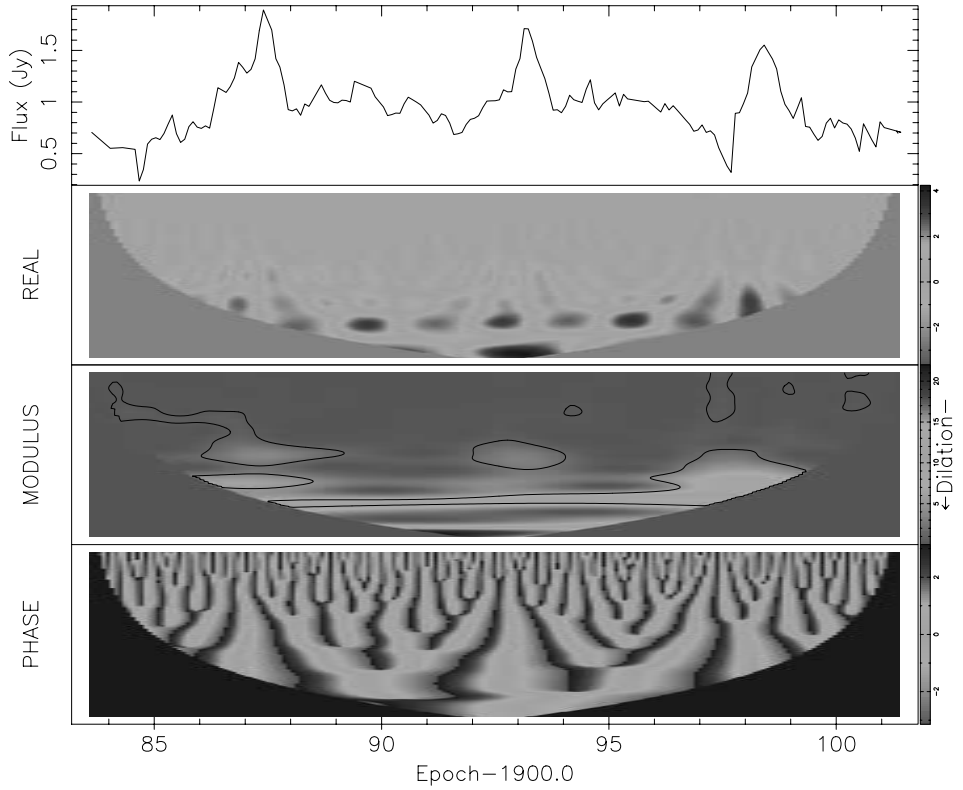


FIG. 10*a*

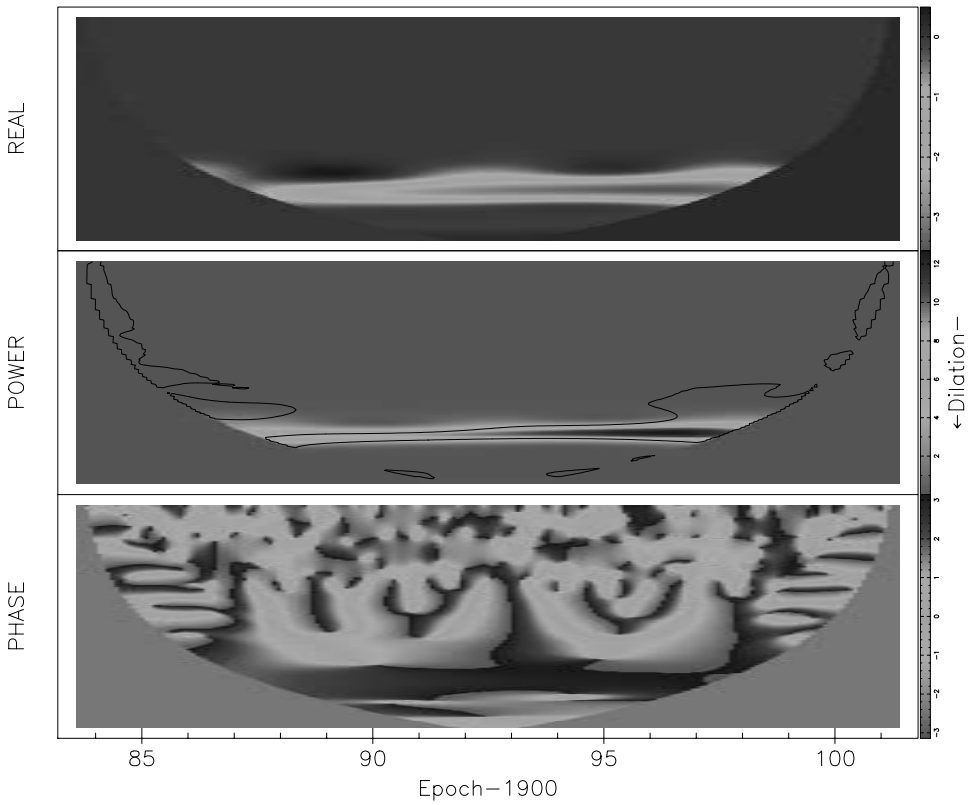


FIG. 10*b*

FIG. 10.—(*a*) Continuous wavelet transform for 0804+499 at 4.8 GHz. The periodic behavior is easily seen as repetition in the real plot. The modulus plot shows the significance of the behavior; particularly notable is the ~2.7 yr period. (*b*) Cross-wavelet transform for 0804+499 at 4.8 GHz with an analyzing signal of period $\tau_n = 2.86$ yr. The data are well correlated with a sinusoid of this period, as is evidenced by the uniformity in the cross-wavelet plots. The contours on both power plots are for the 90% confidence level for correlated noise, assuming a lag-1 autocorrelation of $\alpha = 0.913$. [*See the electronic edition of the Journal for a color version of this figure.*]

respect to source type, and Figure 9 shows histograms for the number of characteristic periods found with respect to source type, binned every 0.25 yr. Out of 30 total sources with sufficient data, 18 were quasars, four were galaxies, and eight were BL Lac objects. A little over half of the sources showed evidence for quasi-periodicity in at least one observing frequency. Column (6) shows the ratio of recorded timescales to individual time series, which gives an idea of the average number of timescales per source. For instance, if three quasars had sufficient data and these quasars had eight individual time series between them over all the observing frequencies, with five of these individual time series exhibiting QPVs, then the ratio of recorded characteristic periods to individual time series would be 5/8 for quasars. A value of 0.33333 would mean that on average most of the sources for this particular type showed evidence for one characteristic timescale over the three observing frequencies, and two timescales over three observing frequencies for a value of 0.66667. As can be seen from the table, on average there was about a little more than one characteristic period observed for every three observing frequencies for all sources. The last column gives the ratio of sources with quasi-periodic behavior in more than one observing frequency to the total number of quasi-periodic sources. Roughly half of the quasi-periodic sources exhibit quasi-periodicity across more than one observing interval. It appears that quasars exhibit characteristic timescales more frequently than BL Lac objects, since about two-thirds of the QSOs showed QPVs, while only about one-third of the BL Lac objects did; however, all of the BL Lac objects showing QPVs repeated the behavior in more than one observing frequency, while only half of the quasars did. This may well reflect the fact that the BL Lac objects of the PR survey sources generally have flat spectra (H. D. Aller et al. 2003, in preparation). In addition, there does not appear to be a distinction among optical classes regarding the length of the timescales. Among sources showing QPVs in more than one observing frequency, the characteristic timescales were similar among the different observing frequencies. However, it is difficult to perform a complete statistical analysis of quasi-periodicity with respect to source type, since only 30 sources were analyzed. In addition, there does not appear to be a distinct relationship between timescales and observing frequency: characteristic timescales do not consistently lengthen with increasing observing frequency, or vice versa. The plots of one particularly promising source for periodic behavior, the quasar 0804+499, can be seen in Figures 10 and 11 at an observing frequency of 4.8 GHz.

Comparing the results for the PR sources with the results expected for correlated noise (§ 4), we find it unlikely that most of the PR sources with characteristic timescales are exhibiting behavior that can be attributed to an AR(1) process. If the time series for the PR sources were the result of AR(1) processes, we would expect the ratio of recorded timescales to time series, Q_t/T, to be $\sim$0.1, since we record characteristic timescales at or above the 90% confidence level. However, as can be seen in Table 2, $Q_t/T = 0.42$.

The lack of uniform quasi-periodic behavior across observing frequencies is unexpected for some of the sources with flat spectra. We have explored the light curves for these sources and conclude that, while generally flat, they do

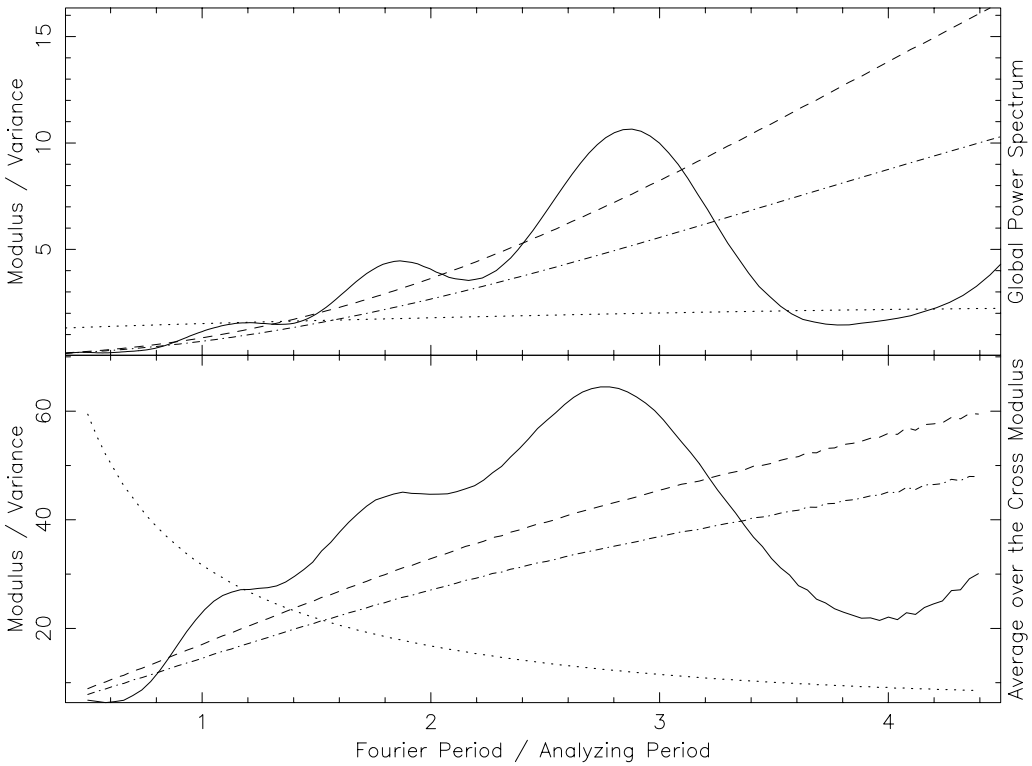


FIG. 11.—Global power spectrum $\tilde{f}^2_{\rm AG}(l_j)$ and the average cross power $\bar{F}_c(\tau_n)$ for 0804+499 at 4.8 GHz. The three peaks corresponding to the three timescales seen in Fig. 10*a* are seen in both plots. The $\sim$2.7 yr timescale is the most prevalent, as expected from visual inspection of the continuous plot. Also shown are the confidence levels for correlated and white noise.

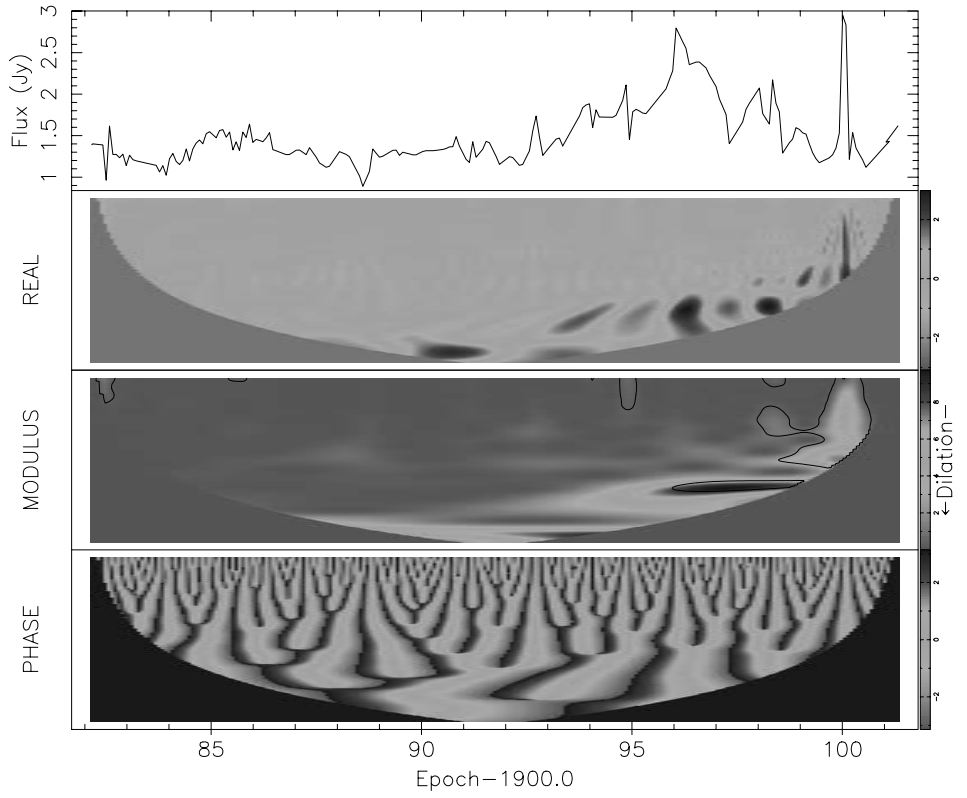


FIG. 12*a*

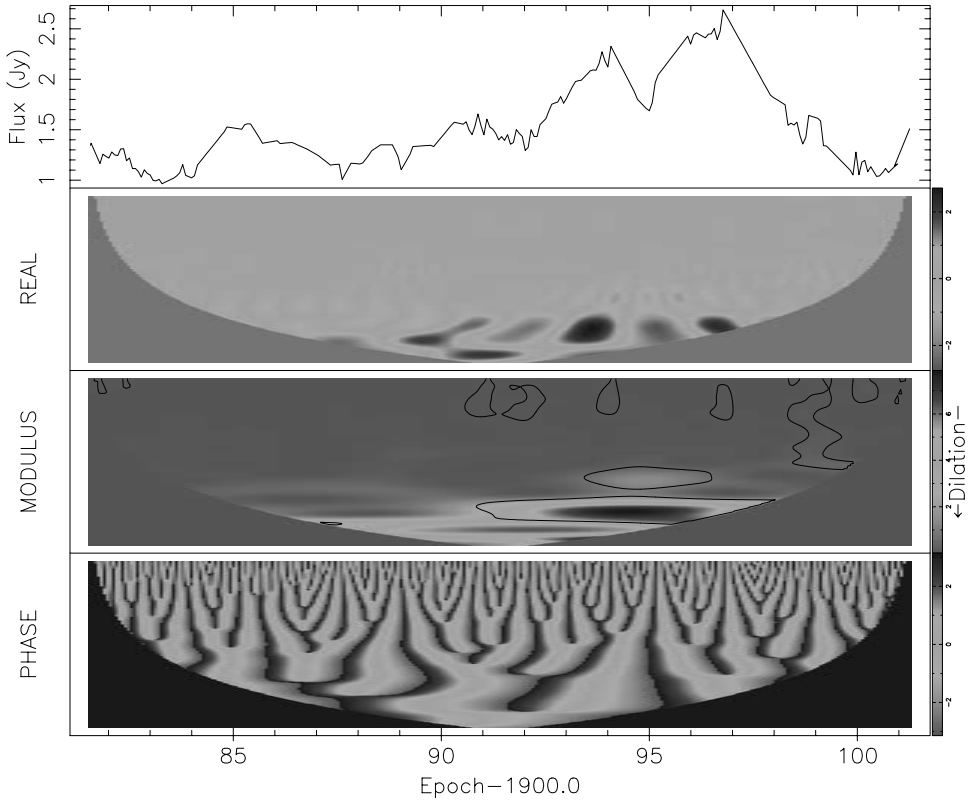


FIG. 12*b*

FIG. 12.—(*a*) Continuous wavelet transform for the BL Lac object 1823+568 at 8.0 GHz. The contours are the 90% confidence level for an AR(1) process of $\alpha = 0.864$. Note the significant behavior seen after 1990. (*b*) Continuous wavelet transform for 1823+568 at 14.5 GHz. The contours are the 90% confidence level for an AR(1) process of $\alpha = 0.987$. One can see that power is distributed over a broad range in scale for this plot, centered about a dilation corresponding to a timescale of $\sim$3.3 yr. Although the two time series share similarities, there are enough differences to account for the varying behavior seen in the transforms. [*See the electronic edition of the Journal for a color version of this figure.*]

exhibit behavior that is different across the three frequencies. Localized activity is sufficient to remove or significantly weaken evidence for quasi-periodic behavior during that time interval, and if quasi-periodic behavior was noted at earlier or later times, it often did not span enough cycles (around four) to warrant recording a characteristic timescale. Typically, such events are not sufficient to affect the average spectral index; however, they can result in changes in the small-scale structure of the light curves, which is detected by the wavelet technique. As an example, Figure 12 shows the continuous transforms for 1823+568 at 8.0 and 14.5 GHz, and the wavelet power spectra are shown in Figure 13. Although the light curves appear similar, the continuous transforms show behavior that is different between the two observing frequencies. Comparison with the power spectra and the continuous plots explains the discrepancy: the transform for the 8.0 GHz curve exhibits a transient timescale of ~2.0 yr, seen after ~1993, whereas the 14.5 GHz curve exhibits a longer timescale of ~3.3 yr that persists throughout the time window. We address the lack of common characteristic timescales with respect to observing frequency further in § 7.

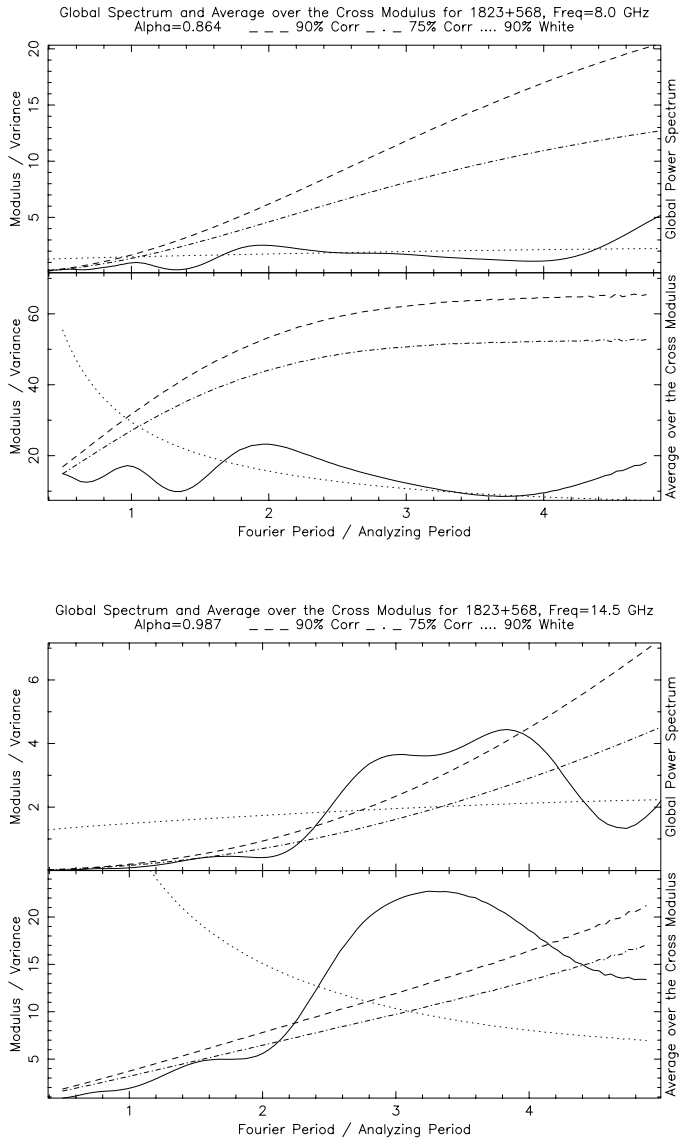


FIG. 13.—Global power spectrum $\tilde{f}^2_{\rm AG}(l_j)$ and the average cross power $\bar{F}_c(\tau_n)$ for 1823+568 at 8.0 GHz (*top two panels*) and 14.5 GHz (*bottom two panels*). Although the ~2.0 yr timescale activity seen post-1990 in the continuous transform for the 8.0 GHz data is significant (see Fig. 12*a*), these plots show that the source does not globally show any behavior in 8.0 GHz that is not inconsistent with an AR(1) process. For the 14.5 GHz data, power is shared over a broad range in scale in both $\tilde{f}^2_{\rm AG}$ and $\bar{F}_c(\tau_n)$; however, the cross transform smooths the two peaks seen in the global spectrum into one distinct peak. The single-timescale interpretation given by the cross technique is visually reinforced in the continuous plot (see Fig. 12*b*).

In addition, we also note that for the 14.5 GHz data for 1823+568 the global wavelet spectrum $\tilde{f}^2_{\rm AG}(l_j)$ and the average cross power $\bar{F}_c(\tau_n)$ differ in assigning a timescale. The global spectrum reveals evidence for two timescales, one at ~2.9 yr and the other at ~3.8 yr, while the average cross power shows evidence for a timescale at ~3.3 yr. Comparison between the two leads us to conclude that the characteristic timescale seen in the plot of $\bar{F}_c$ is more accurate. The global wavelet spectrum shows a broad spread of power between the two timescales, where the timescales are inferred from the somewhat poorly resolved peaks. The average cross power plot also shows a broad spread of power, but with only one peak. This behavior is similar to what was described in § 5.2 for the case of white noise: because the cross-wavelet technique smooths in dilation as well as in translation and acquires information regarding timescales from the analyzing time series, it smooths the two poorly resolved peaks in the global wavelet spectrum into one broad peak. Analyzing the continuous plot, we see that the plot of $\bar{F}_c$ better represents the behavior seen in the continuous transform, since power appears to be shared among a range of scales of ~1.0 yr rather than two distinct timescales separated by about a year. It is more appropriate to assign one characteristic timescale in this case rather than two. Behavior similar to what is seen in the 14.5 GHz data was seen in the 4.8 GHz data as well, but with less significance.

A comparison of the results from Table 1 with those from the structure function analysis performed by Hughes et al. (1992) finds broad agreement, in the sense that most of the sources that we find to have characteristic timescales also exhibited timescales in the structure function analysis, and likewise for those sources lacking timescales. After comparing the timescales from the structure function analysis for those sources that had timescales short enough to meet our requirement of four repetitions over the time window (i.e., shorter than 4–5 yr for most sources), we find that many of the timescales we find are comparable to those found from the structure function analysis. For instance, we deduce a timescale of ~2.6 yr for the source 0836+710 at 4.8 GHz, while the structure function finds that the time series for this source is not correlated above a timescale of 2.88 yr; also, we find a characteristic timescale of ~2.0 yr for the BL Lac object 1803+784, and the structure function analysis gives a timescale of 1.86 yr. Although the structure function analysis gives a measure of the timescale above which variations appear to be uncorrelated, which is not the same as the timescale that we measure, we find that the results from the cross-wavelet technique agree with those from the earlier structure function analysis of Hughes et al. (1992).[1]

[1] Color postscript plots for the continuous and cross-wavelet transforms, as well as the plots for the global wavelet spectrum and the average cross power, are available for all sources from the UMRAO Web site at http://www.astro.lsa.umich.edu/obs/radiotel/prcwdata.html.

7. CONCLUSIONS

We conclude that, complemented with the continuous wavelet transform, the cross-wavelet technique can be an effective tool in the search for quasi-periodicity of a time series. Comparing the results for the Pearson-Readhead survey sources with that expected for a correlated noise process of the form AR(1), we conclude that the observed quasi-periodic behavior is unlikely to be the result of an AR(1) process, since about 40% of the time series for the PR sources had characteristic timescales, compared to about 10% expected for an AR(1) process. The observed timescales may be the result of a type of correlated noise that is not AR(1), and it certainly may not even be stationary noise. However, even if the QPVs arise from correlated noise, it is meaningful to explore the characteristic timescale of a time series, and such results provide a useful diagnostic of the underlying variations.

After applying the cross-wavelet algorithm to the PR VLBI survey sources, analysis revealed evidence for quasi-periodic variations in $\sim$57% of the sources, as well as evidence that $\sim$67% of quasars, $\sim$38% of the BL Lac objects, and 50% of the galaxies have quasi-periodic behavior in at least one observing frequency. The sources were observed to have a mean characteristic timescale of 2.4 yr, with standard deviation of 1.3 yr.

Because the analyzed radio-band variations for the PR sources originate in parsec-scale jets, perturbations that propagate at c will lead to observable fluctuations if they span the flow, guaranteeing timescales on the order of years. In addition, coherent perturbations that arise from the excitation of certain modes of oscillation of the flow, which could give rise to quasi-periodic behavior with timescales comparable to the dynamical response time of the flow (i.e., years), have been shown to arise quite naturally (Hardee et al. 2001). We conclude that our results are in good agreement with the characteristic timescales that we would expect to observe based on the nature of these objects.

There is a transition region where the jet changes from optically thick to optically thin, with optical depth $\tau = 1$ (Cawthorne 1991). Because this region varies with the observing frequency, we are looking at a different physical location in the jet at each observing frequency. It is likely that the timescale of quasi-periodic variations is dependent on their location in the jet. Naively, we would expect to probe larger scale regions with longer characteristic timescales, the lower the observing frequency chosen. The results of our analysis certainly find no such correlation of timescale and frequency. However, jets may accelerate because of adiabatic expansion or decelerate because of entrainment, leading to a change in bulk Lorentz factor with position. In addition, curvature is now known to be a common feature of these flows. A change in flow speed and/or flow orientation with respect to the observer can lead to a significant change in Doppler factor and thus to the observed timescale of activity, masking any simple trends. Furthermore, local jet properties and ambient conditions play a major role in determining what modes of the flow exist and may be excited, and observations that probe different physical scales might well reveal activity in one frequency band but not in another.

Although the number of sources analyzed here is in no way exhaustive, we see no reason why such quasi-periodic behavior should be confined to the PR survey sources, and we find it likely that many active galactic nuclei exhibit quasi-periodicity. Only four galaxies had sufficient data for analysis and so are tabulated but not discussed. A statistical analysis on the results of applying the cross-wavelet technique to a greater number of sources would lead to a more interesting and conclusive comparison of quasi-periodic behavior and source type, as well as evidence for quasi-periodicity in active galactic nuclei in general. In addition, the cross-wavelet transform may also be a useful tool for analyzing the correlation of a source between different observing frequencies.

We would like to thank the anonymous referee for many helpful and insightful comments that contributed to the significant improvement of this manuscript.

REFERENCES

Aller, H. D., Aller, M. F., Latimer, G. E., & Hodge, P. E. 1985, ApJS, 59, 513
Aller, M. F., Aller, H. D., & Hughes, P. A. 2003, ApJ, 586, 33
Cawthorne, T. V. 1991, in Beams and Jets in Astrophysics, ed. P. A. Hughes (Cambridge: Cambridge Univ. Press), 187
Farge, M. 1992, Ann. Rev. Fluid Mech., 24, 395
Hardee, P. E., Hughes, P. A., Rosen, A., & Gomez, E. A. 2001, ApJ, 555, 744
Hughes, P. A., Aller, H. D., & Aller, M. F. 1992, ApJ, 396, 469
———. 1998, ApJ, 503, 662
Kyprianou, A., & Staszewski, W. J. 1999, J. Sound Vibration, 228, 199
Lehto, H. J. 1999, in ASP Conf. Ser. 159, BL Lac Phenomenon, ed. L. O. Takalo & A. Sillanpää (San Francisco: ASP), 257
Ott, M., Witzel, A., Quirrenbach, A., Krichbaum, T. P., Standke, K. J., Schalinski, C. J., & Hummel, C. A. 1994, A&A, 284, 331
Pancheva, D., Mukhtarov, P., Mitchell, N. J., Beard, A. G., & Muller, H. G. 2000, Ann. Geophys., 18, 1304
Percival, D. P. 1995, Biometrika, 82, 619
Roy, M., Papadakis, I. E., Ramos-Colón, E., Sabruna, R., Tsinganos, K., Papamastorakis, J., & Kafatos, M. 2000, ApJ, 545, 758
Torrence, C., & Compo, G. P. 1998, Bull. Am. Meteorol. Soc., 79, 61